

The spectrum of SC45 5Cu bulk shows the lack of copper crystalline phase replaced by presence of an iron oxide containing Cu, in fact peaks at 31,28 and 40,2 and 55,2 2θ angles is identified as copper iron oxide which stabilized it in a crystalline phase.

#### 7.2.4. Quantitative evaluation of magnetite present into the doped glass ceramics

The percentage of magnetite, present in each glass ceramics, was evaluated from the saturation magnetization values of each sample. The following formula was used:

$$\% Magnetite = \frac{Ms_{SC45Ag}}{Ms_{Magnetite}} * 100$$

$$\% Magnetite = \frac{Ms_{SC45Cu}}{Ms_{Magnetite}} * 100$$

Where :

$Ms_{SC45Ag}$  [ $A\ m^2/kg$ ]: saturation magnetization value of silver doped glass ceramics. This parameter provides the amount of magnetic material present in the samples and it is extrapolated by hysteresis cycle at 800 kA/m.

$Ms_{Magnetite}$  [ $A\ m^2/kg$ ]: saturation magnetization of pure Magnetite taken as a standard. It was chosen for the quantification of magnetite into the glass ceramic samples.

$Ms_{SC45Cu}$  [ $A\ m^2/kg$ ]: saturation magnetization value of copper doped glass ceramics.

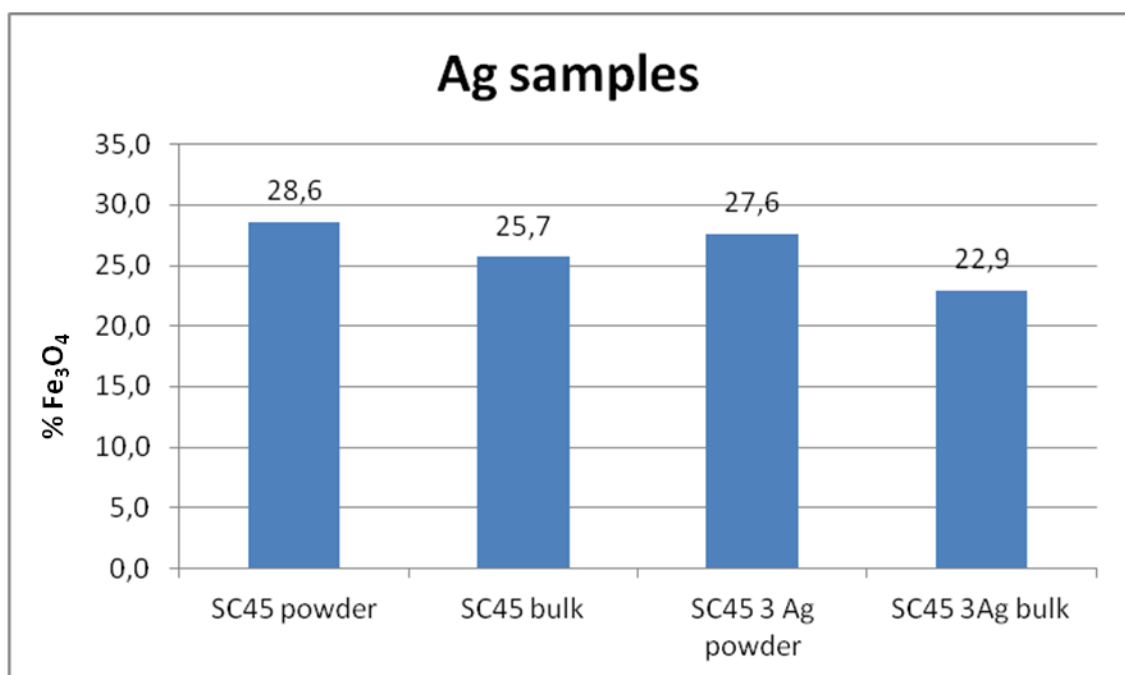


Figure 7.22: Amount of magnetite in the silver-doped glass-ceramics respect to the control sample SC45 powder and SC45 bulk

## Results and Discussion Antibacterial characterization of SC45

Figure 7.22 reports the calculated percentages of magnetic phase into the control and silver doped glass ceramics. SC45 3Ag powder presents a value of magnetite very close to the SC45 powder and the same trend is seen for the SC45 3Ag bulk compared to the SC45 bulk. The presence of silver does not modify in a significant way the quantity of magnetite respect to the control both in powder and after annealing treatment. A little decreasing trend is observed between SC45 powder and bulk samples and the same with SC45 Ag samples. The data are not significantly different.

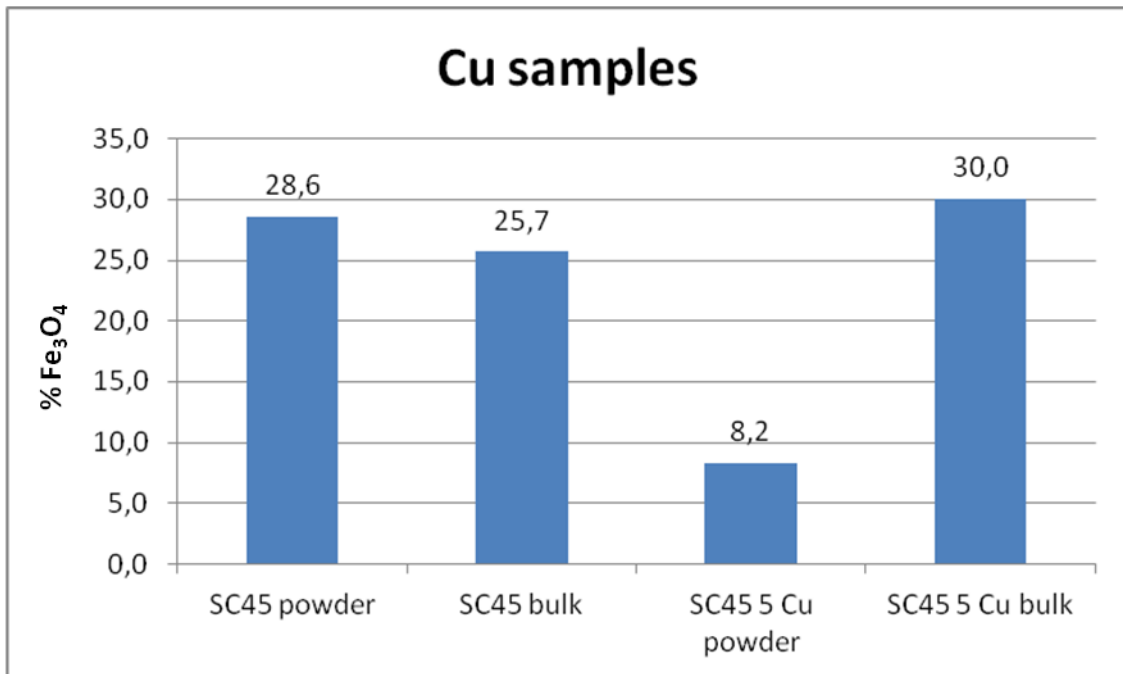


Figure 7.23: Amount of magnetite in the copper-doped glass-ceramics respect to the control sample SC45 powder and SC45 bulk

Figure 7.23 reports the amount of magnetic phase into the copper doped glasses. The value of magnetite into the SC45 5Cu power is lower than the SC45 powder. Copper could form a ionic solution that inhibits the magnetic phase. In this sample the copper has a lot of unsaturated bonds which can interact with magnetite in a negative way. When the sample was annealed, the formation of a copper iron oxide is seen in XRD analysis (Figure 7.21 blue line), this phase is stable and saturates the copper bond. So the antiferromagnetic effect disappeared, in fact the glass ceramic recovers its magnetic and thermal properties. In this case it seems that the annealing treatment provided enough energy to form a more stable copper compound.

## 7.2.5. Evaluation of magnetic parameters at 800 kA/m

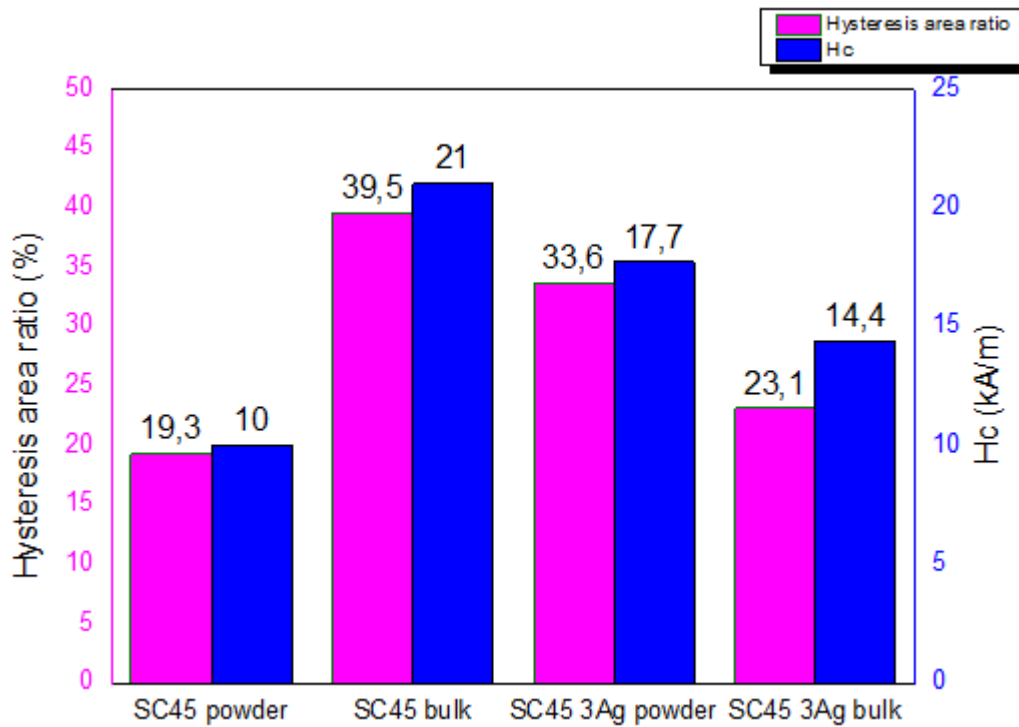


Figure 7.24a: Hysteresis area ratio and coercive field at a maximum applied magnetic field of 800 kA/m of control and silver doped glass ceramic

The hysteresis area ratio and the coercive field values of SC45 and silver doped samples at 800 kA/m are shown in figure 7.24a. All the values are normalized respect to the magnetite hysteresis cycle, here not reported, which represents the maximum amplitude of the cycle.

The hysteresis area of the control samples respect to the silver doped samples were evaluated at a maximum applied magnetic field in correspondence of which the cycle is completely close at the saturation hysteresis.

All the sample possess an elevate capacity of generate heat under the effect of an alternate magnetic field.

## Results and Discussion Antibacterial characterization of SC45

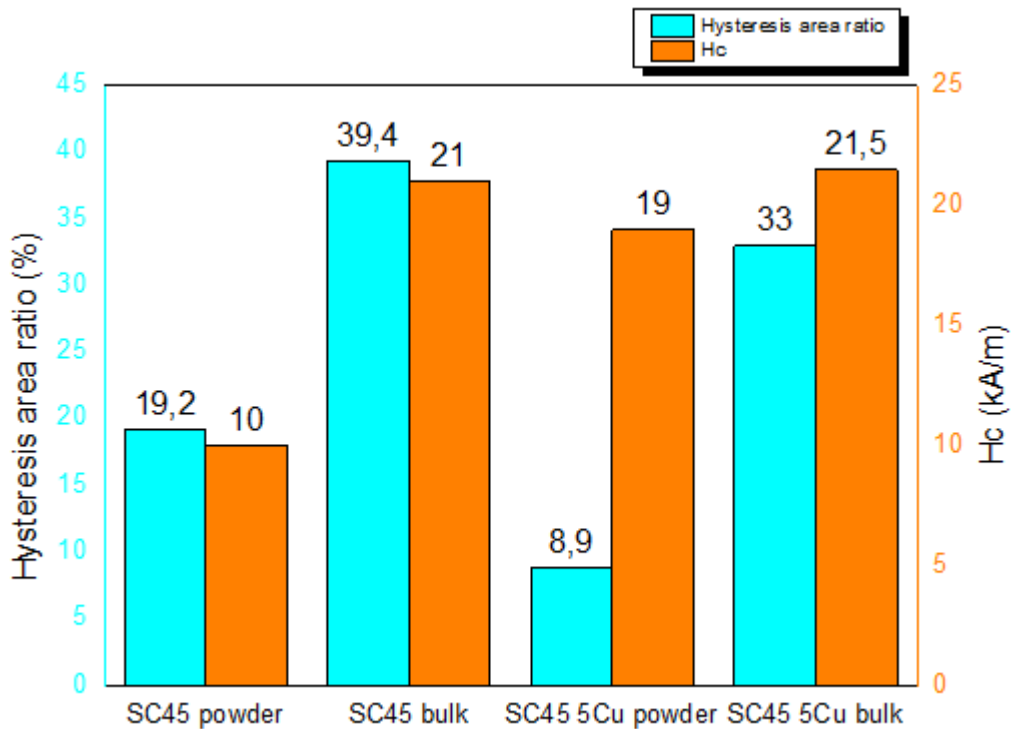


Figure 7.24b: Hysteresis area ratio and coercive field at a maximum applied magnetic field of 800 kA/m of control and copper doped glass ceramic

The hysteresis area ratio and the coercive field values of SC45 and copper doped samples at 800 kA/m are shown in figure 7.24b. The value of hysteresis area ratio of the SC45 5Cu bulk are comparable with value of SC45 bulk. Only the SC45 5Cu powder presented the lowest value of hysteresis area ratio respect to the control. While after the annealing treatment it recover its ferrimagnetic properties.

The microstructure of the samples is quite similar because the Hc value did not undergo to a significative variation a part for the SC45 powder.

For the better understanding of how the copper influence the ferrimagnetic behavior of SC45 a thorough analysis will be necessary if the copper will be choose as the antibacterial agent.

### 7.2.6. Evaluation of magnetic parameters at 34 kA/m

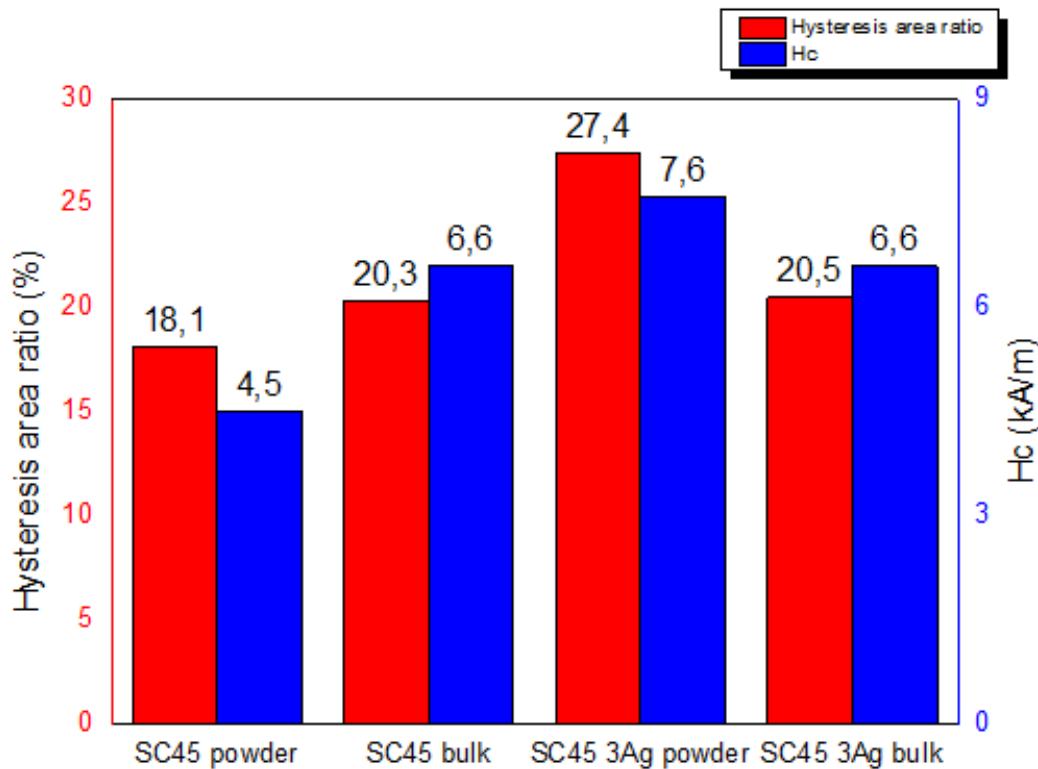


Figure 7.24: Hysteresis area ratio and coercive field at a maximum applied magnetic field of 34 kA/m of control and silver doped glass ceramic

The hysteresis area of the control samples respect to the silver doped samples were evaluated at a maximum applied magnetic field of 34 kA/m in correspondence of which the cycle is not yet close far from the saturation hysteresis. All the values are quite similar and were normalized respect to the magnetite hysteresis cycle, here not reported, which represents the maximum amplitude of the cycle.

The highest data of coercive field was assigned to SC45 3Ag powder which means that the sample had the highest number of microstructural defect and consequently a much higher energy is required to move the magnetic domain walls. So in agreement with this result even the hysteresis energy was higher than the others.

## Results and Discussion Antibacterial characterization of SC45

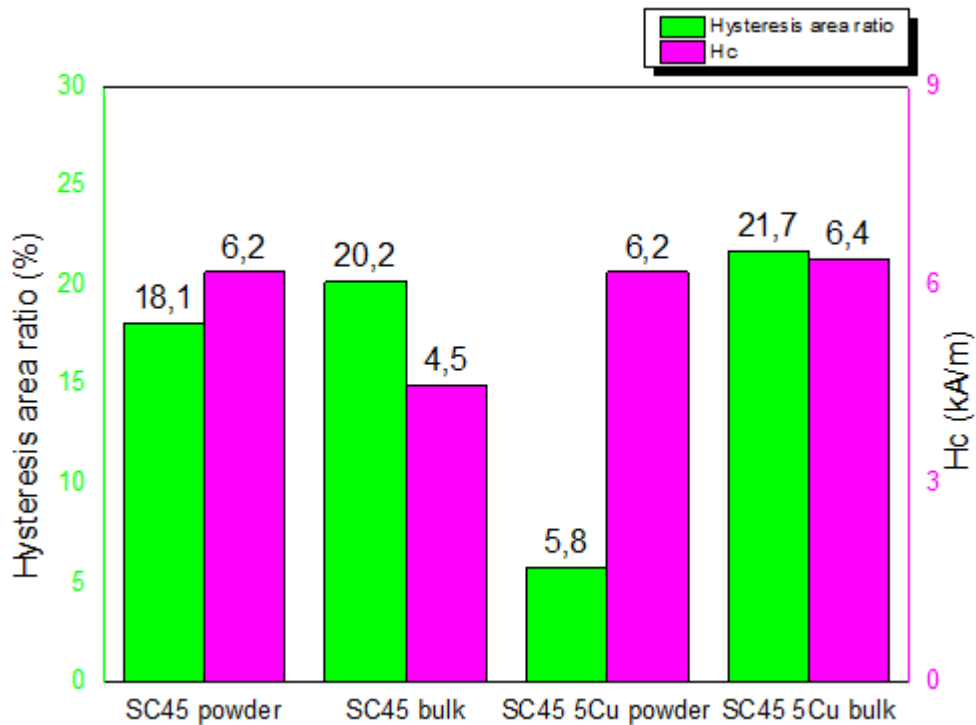


Figure 7.25: Hysteresis area ratio and coercive field at a maximum applied magnetic field of 34 kA/m field of control and copper doped glass ceramic

The hysteresis energy ratio of SC45 5Cu powder decreases of 12,3% respect to the SC45 powder. This is due to an important reduction of magnetite as just evidence in figure 7.25. It could be hypothesized that the presence of copper in an ionic form produced an interaction with the magnetic electronic spin of iron. Consequently copper ion has determined the loss of magnetite magnetic response .

After the annealing treatment of the SC45 5Cu glass ceramic the unfavorable effect disappeared and the hysteresis energy ratio became comparable with the value of SC45 bulk undergone to the same treatment.

The coercive field of SC45 5Cu powder is the same of SC45 powder. Probably the microstructures of the two glasses are very similar.

The  $H_c$  of SC45 bulk is lower than the same value of SC45 5Cu bulk. Heat treatment has probably induced an increase of internal microstructural defects which have generated a higher magnetic area respect to the control sample.

### 7.2.7. Calorimetric tests

The results are reported as a mean value of three recorded temperatures with their standard deviation values.

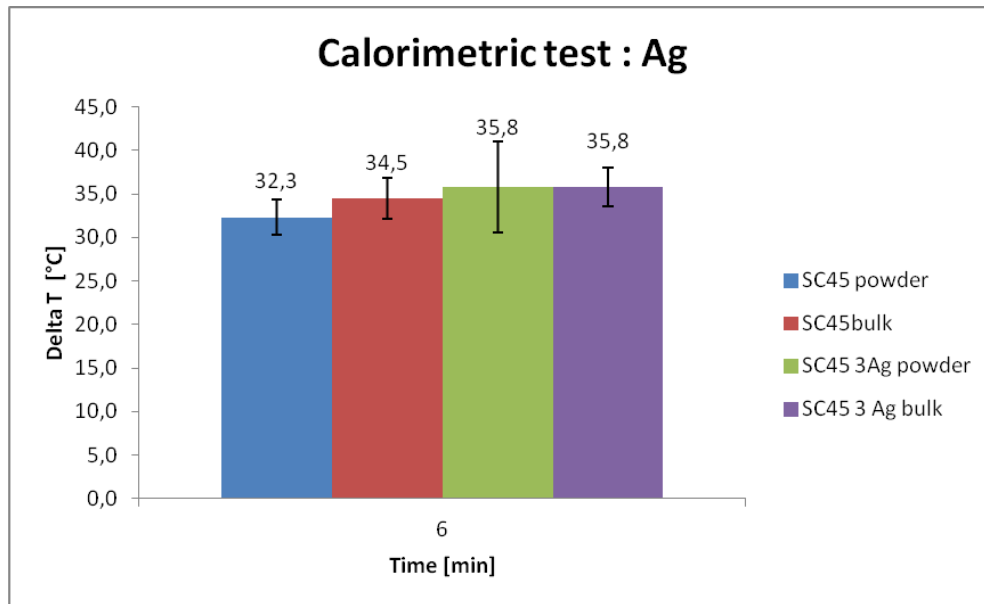


Figure 7.26: Calorimetric measures on SC45 powder, SC45 bulk , SC45 3Ag powder and SC45 3Ag bulk at 22,5 mT after 6 minutes heating

Figure 7.26 reports the calorimetric measures of SC45 3Ag powder and SC45 3Ag bulk respect to the controls samples SC45 powder and bulk. After 6 minutes of heating the increasing temperature of all samples is comparable. The results are coherent with the hysteresis measures at low magnetic field. Taking into account the error bar of each sample, the annealing effect does not play a significant role with silver as a dopant agent for SC45 in term of heating generation.

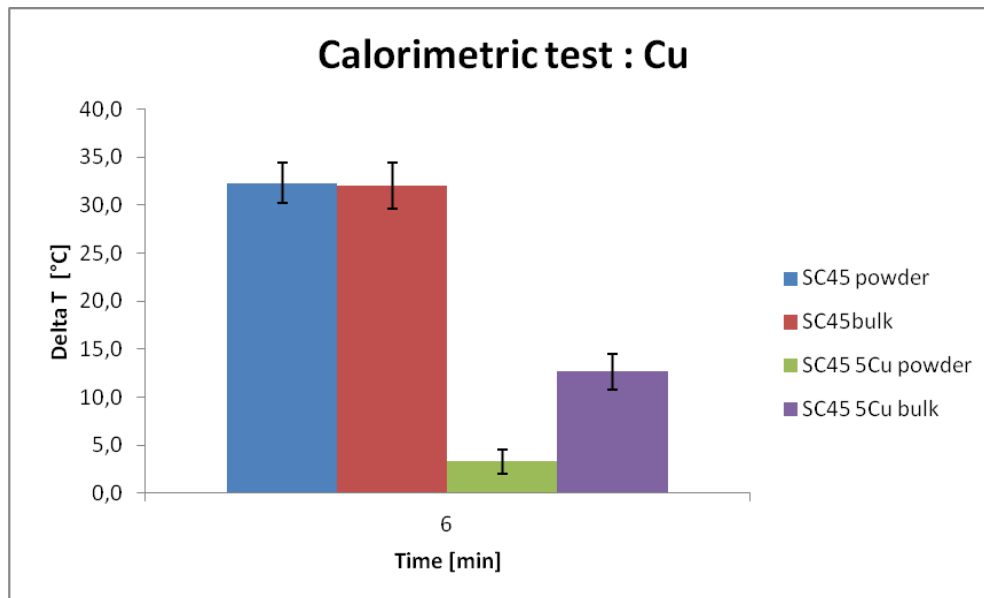


Figure 7.27: Calorimetric measures on SC45 powder, SC45 bulk, SC45 5Cu powder and SC45 5Cu bulk

Figure 7.27 reposts calorimetric measurements of SC45 powder and bulk and, SC45 5Cu powder and bulk.

The bulk and the powder controls (i.e. un-doped glass-ceramic) express a high increasing temperature respect to the copper doped glasses.

The SC45 Cu with no annealing treatment presents very low heating capability, the presence of Cu seems to reduce the magnetic properties of magnetite. During the performance of the test the temperature of the water increase only of 3,3 °C with a decreasing of 89% respect to the powder control sample. This effect is less evident with the bulk material. In fact it regains ability to generate heat under the effect of an alternate magnetic field but without reaching the temperature increase of the bulk control, even if it has the same quantity of magnetite of the SC45 bulk.

Probably, in the powder sample, copper ions modify the crystallographic structure of magnetite even without change the phase.

From XRD analysis no crystalline phase containing copper is detected but probably the unsaturated copper bonds generated the interaction with iron ions in the magnetite. The final effect can be induced by suppression of ferromagnetic behaviour due to the antiferromagnetic coupling with the copper ions. Therefore the material is not able to generate heat under the effect of an alternate magnetic field.

The theoretical approach in the correlation of calorimetric measurements and hysteresis area confirms that wider the hysteresis loop is and bigger will be the increasing temperature

independently from the working frequency, as demonstrated by impedance tests with the composites materials. The frequency stimulation between kHz up to 10 MHz does not influence the heating generation mechanism of samples. The heating ability will be proportional to the quantity of magnetic material and time exposure to the alternate magnetic field up the resonance phenomena. The resonance effects would perturb the system and a higher amount of energy could be absorbed by the magnetic field from the samples[10].

### 7.2.8. Specific Power losses

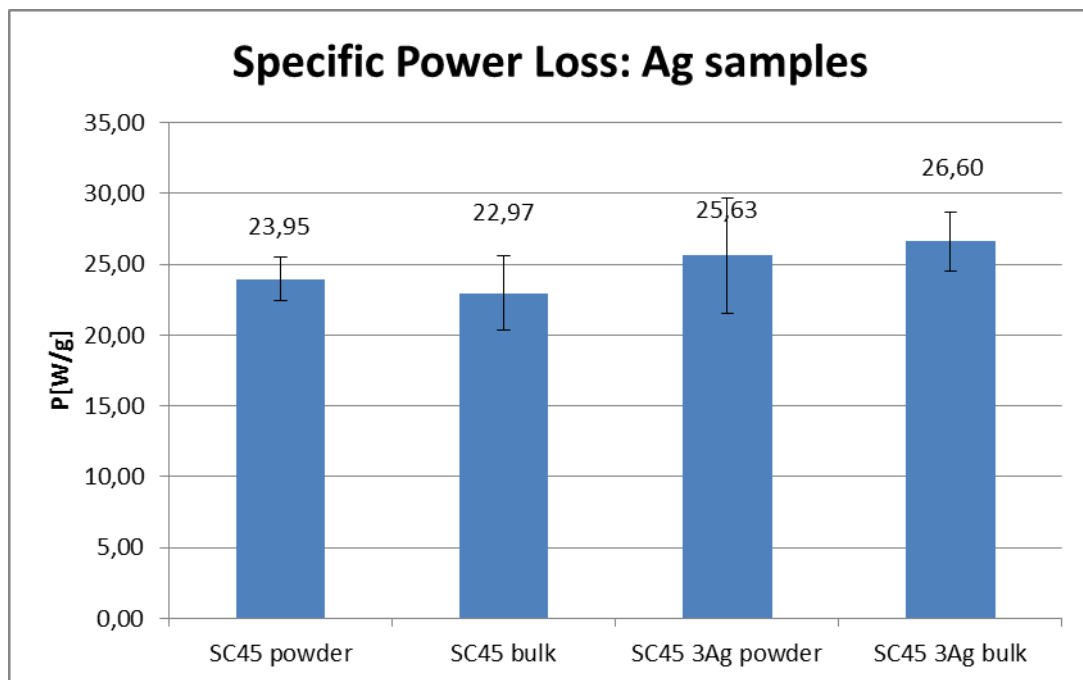


Figure 7.28: Power losses of SC45 powder and bulk respect to SC45 3Ag powder and bulk

Figure 7.28 reports the specific power losses (SPL) of the silver doped glass ceramics respect to the SC45 controls. The trend is in agreement with the calorimetric measures. The SPL is proportional to the heat capacity generate from each samples. The effect of annealing treatment and the addition of silver into the glass ceramic do not modify the power losses respect to the control.

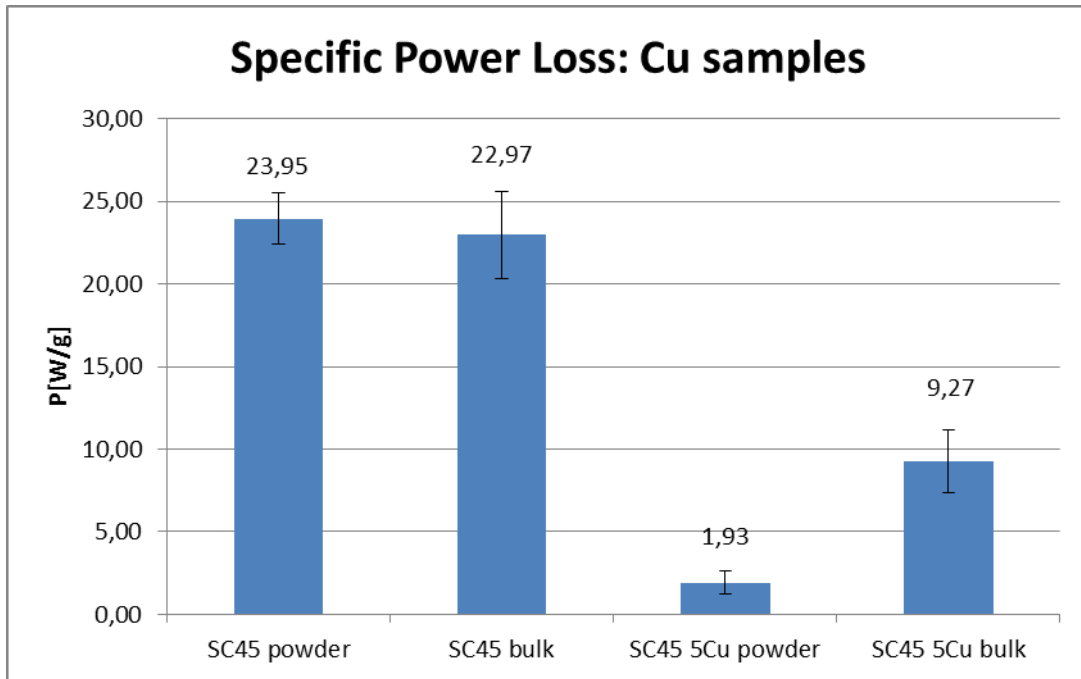


Figure 7.29: Power losses of SC45 powder and bulk respect to SC45 5Cu powder and bulk

Figure 7.29 shows the SPL of copper doped samples in powder and bulk form respect to the control SC45. The SC45 5Cu powder presents a power loss reduction of 92% respect to the control powder. The effect is strictly connected with the reduction of real amount of magnetite into the sample which is related to a reduction of magnetic response as explain before for the calorimetric measures.

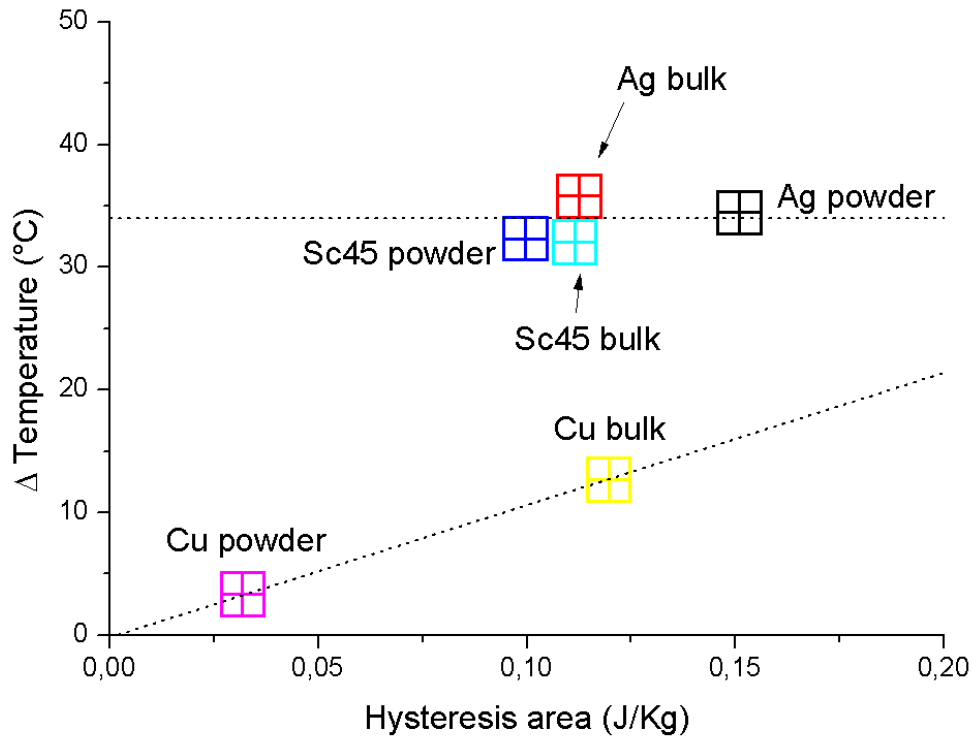


Figure 7.30: Correlation between hysteresis energy losses and increasing temperatures

Figure 7.30 correlates the hysteresis area at low field (34 kA/m) with the increasing temperature of the all samples.

The first consideration regards the different behavior between silver and copper samples respect to the control.

For copper-containing samples the increasing of hysteresis area determines a temperature increase with a linear trend correlation.

For the silver-containing samples the trend is very different, in fact the increase of hysteresis energy between powder and bulk is seen as an unchanged factor respect to the increasing temperature.

### 7.2.9. Antibacterial test

The antibacterial test is performed on the following samples :

1. SC45 bulk identified on the plate as TQ
2. SC45 3Ag bulk on the plate as Ag
3. SC45 5Cu bulk on the plate as Cu
4. SC45 3Ag bulk grinded

## Results and Discussion Antibacterial characterization of SC45

5. SC45 5Cu bulk grinded
6. SC45 powder
7. SC45 3 Ag powder
8. SC45 5Cu powder

The bulk samples were also tested after grinding in order to avoid the differences in surface roughness, and so specific surface area, of the samples. The tested materials are the same used for the previous characterization. All the powder and bulk grinded samples are tested in a tablet form.

The test chosen for this characterization is the method of the inhibition halo (Kirby Bauer-Test). After the preparation of *Staphylococcus aureus* bacterial culture, samples are placed on the plate. The aim is to evaluate the possible formation of an inhibition halo around the sample, index of the material ability to avoid the bacterial proliferation and sample contamination.

Figure 7.31 reports the result of inhibition halo test performed with bulk samples. As it can be observed in figure 7.31 both copper and silver containing samples are not able to create an inhibition halo (figure 7.31b and 7.31c). The light yellow halo around SC45 5Cu sample (figure 7.31c) is not an inhibition halo but is due to the copper diffusion in the agar plate.

## Results and Discussion Antibacterial characterization of SC45

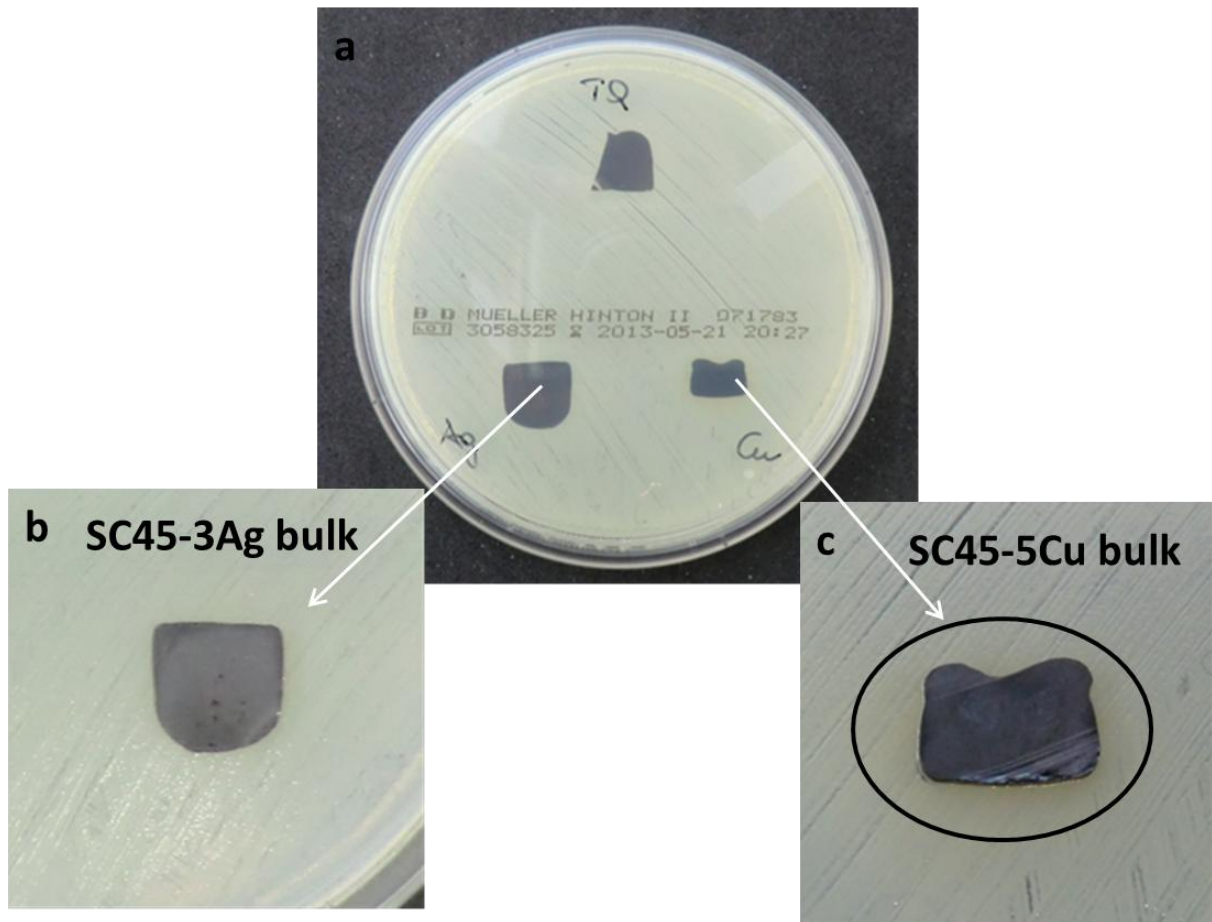


Figure 7.31.: Results of Inhibition halo test- BULK SAMPLES

After performing the Kirby Bauer test, without observing any significant zone of inhibition around the samples, the analysis of the surfaces of the samples in contact with the bacteria is performed by SEM analysis

The samples were passes on a busen in order to kill the bacteria, eventually adhered on sample surface, without alter their morphology.

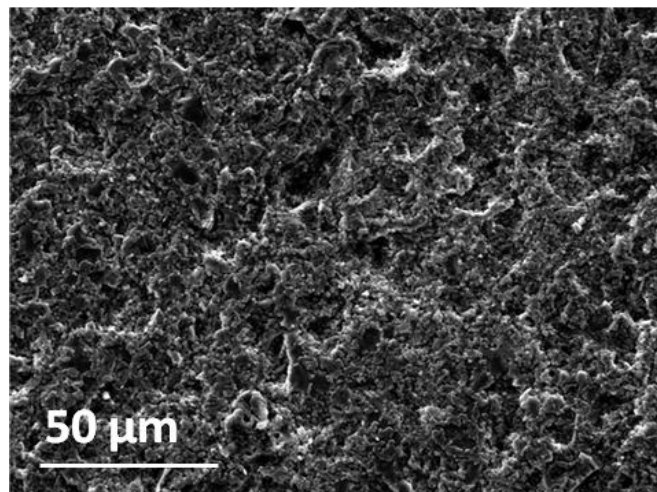


Figure 7.32: SEM image of SC45 bulk surface in contact with bacteria

## Results and Discussion Antibacterial characterization of SC45

Figure 7.32 shows the bacterial colony adhered to the surface of the bulk control sample. Figure 7.32a show an area of SC45 bulk surface completely covered by *Staphylococcus aureus*.

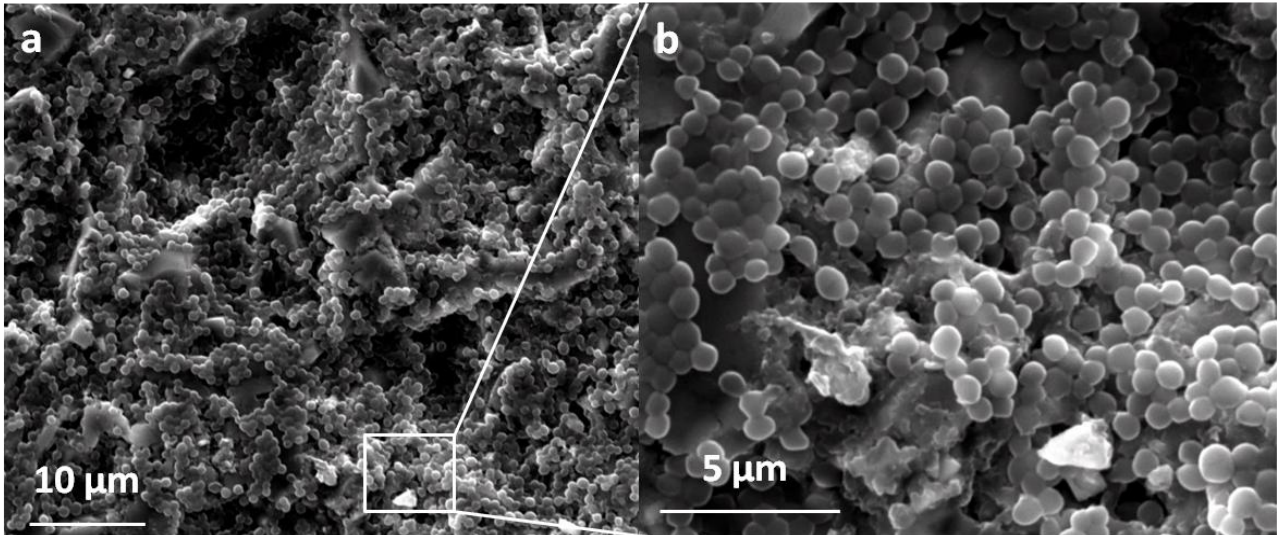


Figure 7.33: SEM image of SC45 bulk surface in contact with bacteria

Figure 7.33a-b show two magnifications where the bacteria are well defined and homogeneous distributed on all the free surface of the bulk control sample.

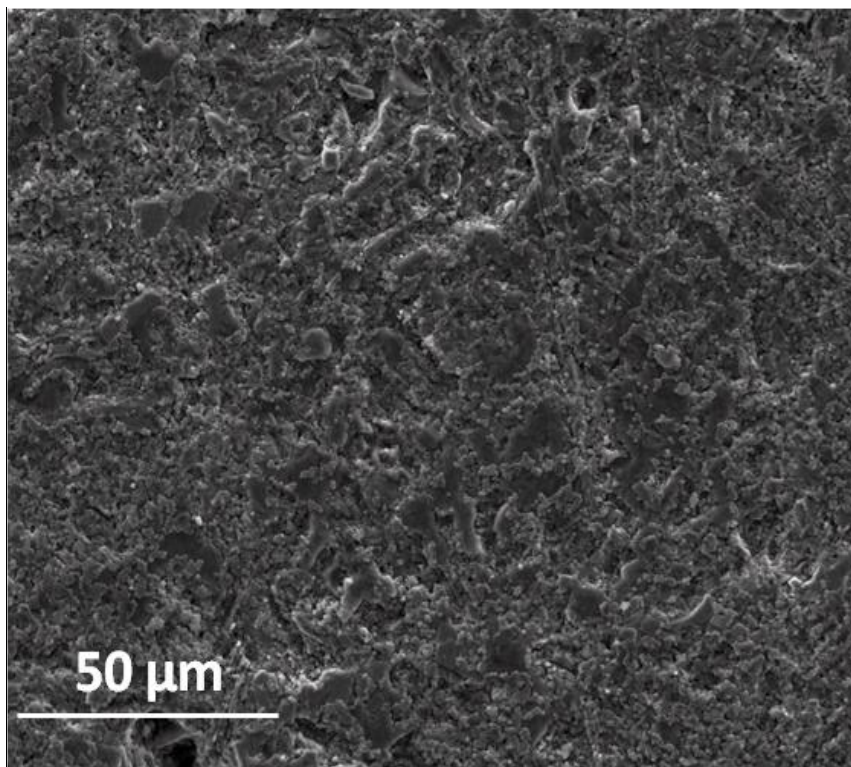


Figure 7.34: SEM image of SC45 3Ag bulk surface in contact with bacteria

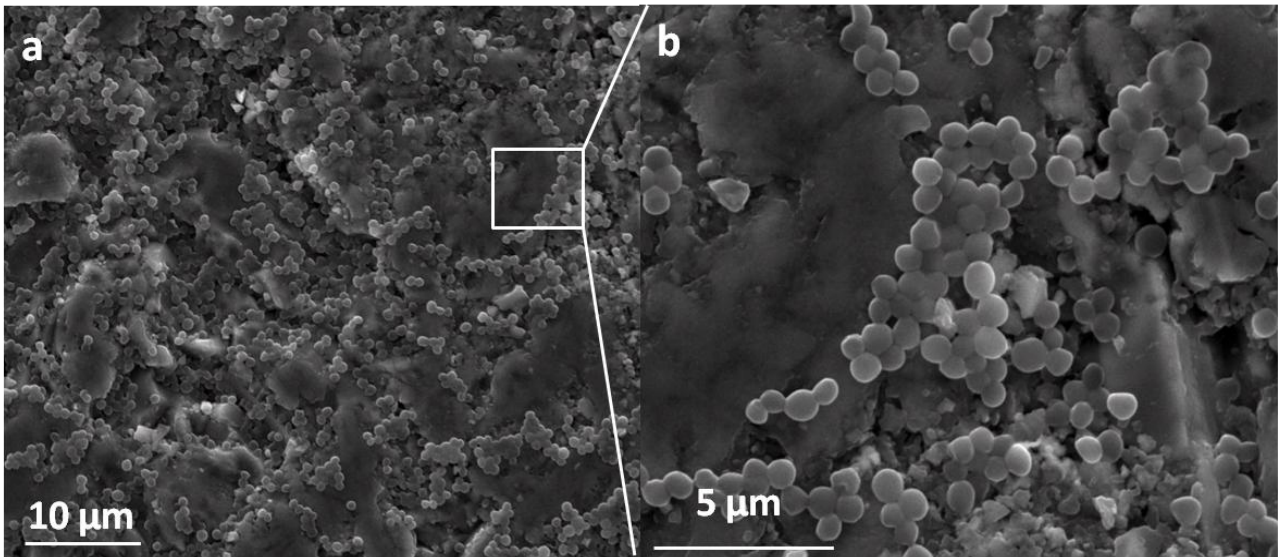


Figure 7.35: SEM image of SC45 3Ag bulk surface in contact with bacteria

Figures 7.34 and 7.35 a-b show the adhesion of bacteria on the SC45 3Ag specimen at 1600x , 5000x (b), 15000x(c). The amount of adhered bacteria seems less respect to the control but the antibacterial activity is not sufficient. The effect of silver is not expressed. Probably the macro particles of metallic silver cannot release a sufficient  $Ag^+$  amount and moreover they do not interact with bacteria membranes. They were able to proliferate and spread on the material surface.

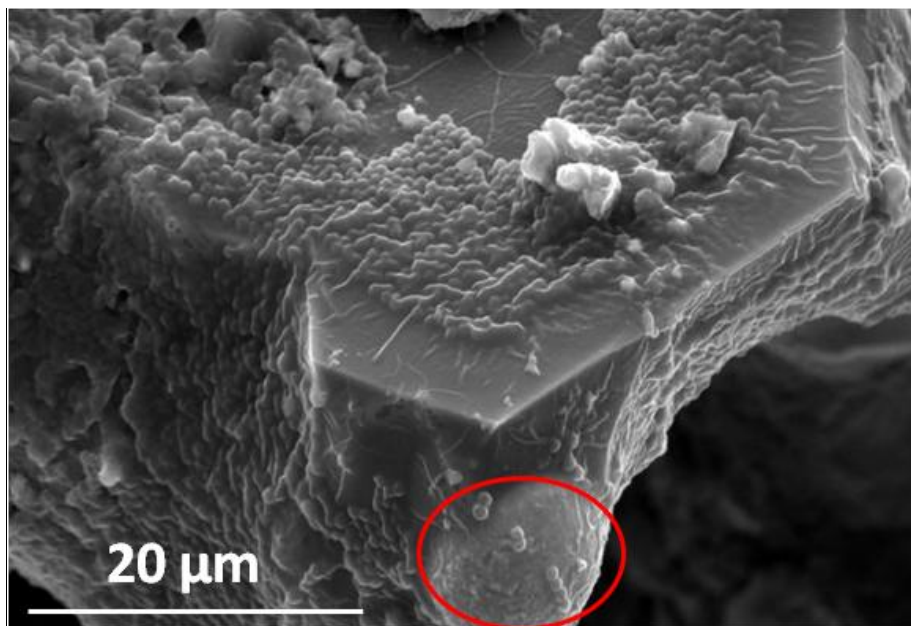


Figure 7.36: SEM image of SC45 3Ag bulk surface in contact with bacteria. In the red circle it is reported a large spherical metallic silver particle.

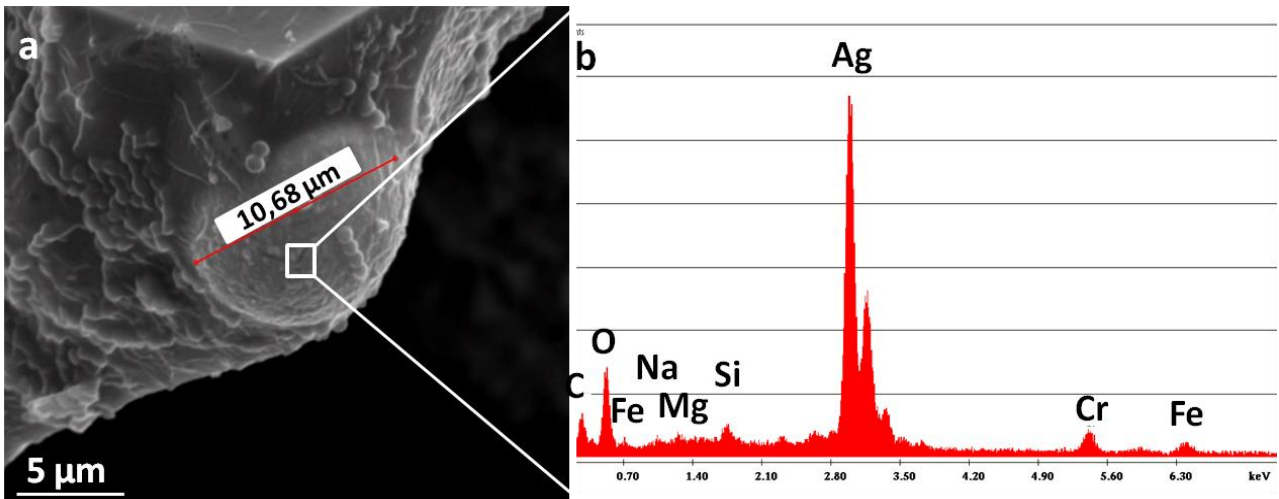


Figure 7.37: SEM image of a metallic silver particle on SC45 3Ag bulk surface in contact with bacteria(a). (b) Compositional analysis of the precipitate

In figure 7.36 is reported a crystal of magnetite that was colonized by bacteria. At the bottom of the image it is clearly visible a very large silver particle with a diameter of 10 μm. Figure 7.37a-c evidences how some bacteria are able to adhere to the metallic particle proving the ineffectiveness of so large crystals. This result evidences the inability of silver particle to release enough ions for the generation of inhibition halo .

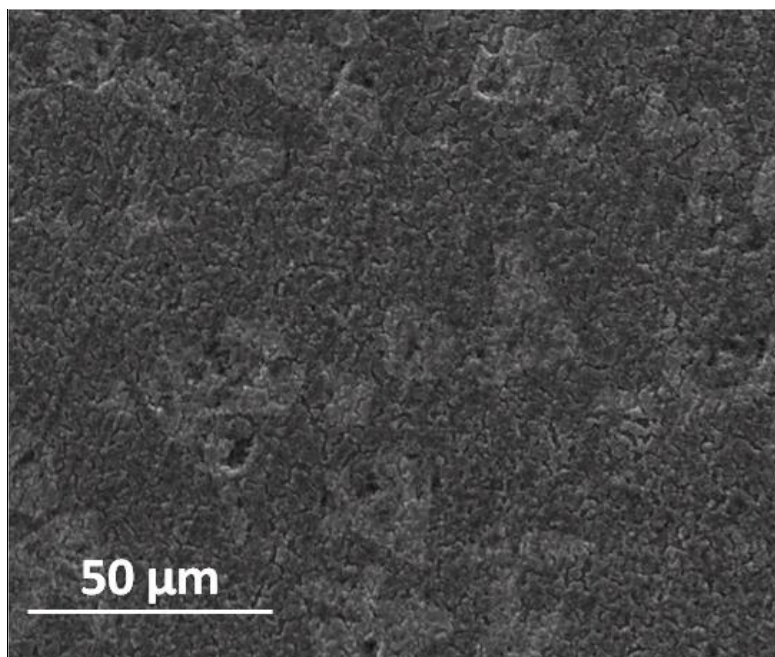


Figure 7.38: SEM image of SC45 5Cu bulk surface in contact with bacteria

## Results and Discussion Antibacterial characterization of SC45

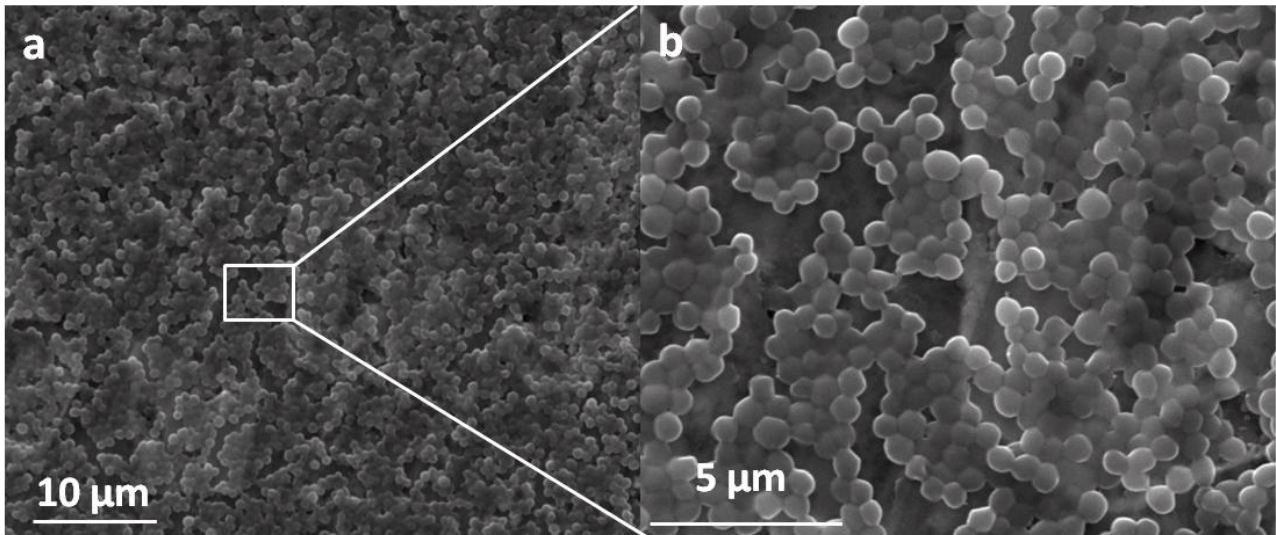


Figure 7.39: SEM image of SC45 5Cu bulk surface in contact with bacteria

Figures 7.38 and 7.39 show three different magnification at 1600x, 5000x , 1500x of SC45 5Cu bulk. It is evidenced the ability of bacteria to adhere on the surface of the specimen. In this sample the amount of copper is low and moreover after annealing treatment it reacts to form a crystalline solids compound. The combination of these two events has confirmed a low release capability of the sample.

The test is repeated with the pulverization and sieve of all bulk samples. The aim is to have a specific surface area similar to powder samples; in this way an eventual influence of thermal treatment can be evidenced.

The samples were produced using 200 mg of doped SC45 powders uniaxially pressed at 4 tons for 10 seconds in order to prepare disks of a diameter of 1 cm and a thickness of 0,5 mm.

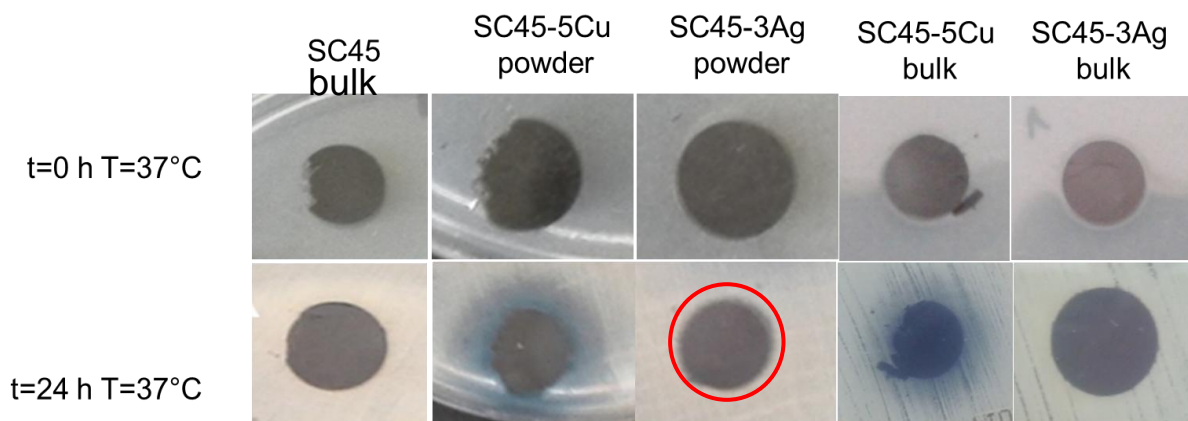


Figure 7.40: Results of Inhibition halo test: powder and bulk grinded samples

The results of antibacterial tests on powder and bulk samples obtained by melting and quenching technique are shown in figure 7.40. The sample SC45 3Ag powder shows a very weak halo around

the sample, the thickness is about 1 mm ( see red circle in figure 7.40). The tested sample powder has a specific surface higher than the bulk sample and then accordingly more reactive towards the release of Ag and subsequent inhibition of bacterial growth.

The sample SC45 5Cu powder develops a behavior very similar to the bulk sample, in fact it seems that there was an antibacterial effect but indeed the copper only diffused out of the sample without producing antibacterial effect. Copper diffuses into the agar and gives it a different color but with bacteria proliferation.

As reported before, the bulk samples were tested even in tablet form in order to have the same surface to volume ratio of the other samples.

The inhibition halo test had not produced any significant results not for SC45 5Cu bulk nor SC45 3Ag bulk.

### 7.2.10. Molten salt ion exchange

#### 7.2.10.1. $\text{NaNO}_3:\text{AgNO}_3$ 100:0,05 mol/mol Ag-2000

In the following section it is reported the FESEM-EDS characterization performed on SC45 Ag2000 after the synthesis process. Morphology of Ag doped SC45 powder, compositional analysis on wide surface and on specific particles and quantitative analysis are performed. This sample contains the lowest amount of silver ions.

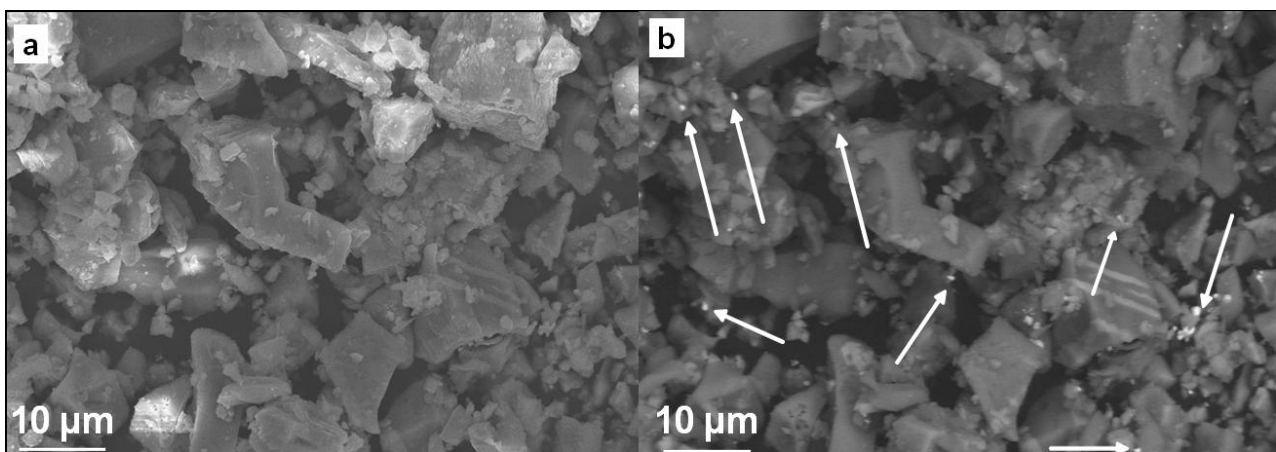


Figure 7.41: FESEM of SC45 Ag2000

Figure 7.41 reports a secondary electron image (a) and backscattering (b) of SC45 particles  $< 20\mu\text{m}$  after the molten salt ion exchange. In figure 7.41b in backscattering modality, white arrows evidence the different brightness of precipitates assigned to metallic silver.

## Results and Discussion Antibacterial characterization of SC45

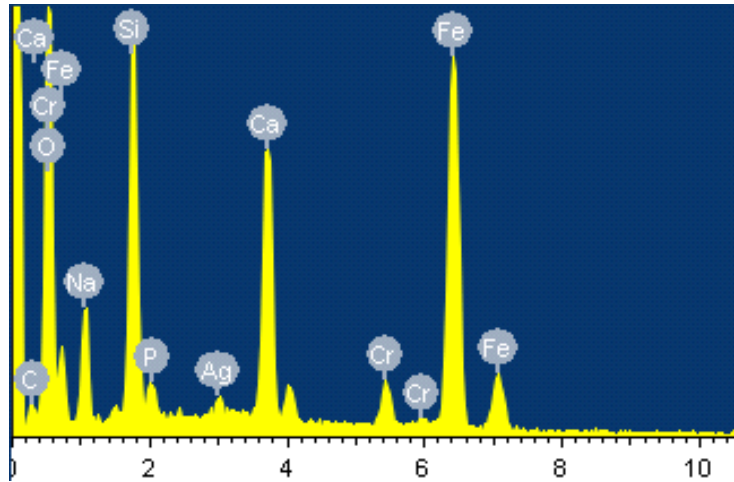


Figure 7.42: compositional analysis of SC45 Ag2000

Figure 7.42 reports the EDS analysis of SC45 Ag2000 glass ceramic with evidence of the presence of silver and chromium (the last one come from the metallization of sample). Silicon, calcium, phosphorus, iron and oxygen are typical of SC45 while silver is introduced with the molten salt ion exchange procedure. The silver peak is quite low because the analysis is performed on a wide area.

	SC45	SC45 Ag2000
	%at	%at
NaK	<b>22,5 ± 0,1</b>	<b>19,5 ± 0,9</b>
SiK	<b>21,3 ± 0,2</b>	<b>22,1 ± 0,8</b>
P K	<b>1,6 ± 0,1</b>	<b>1,7 ± 0,1</b>
CaK	<b>16,5 ± 0,1</b>	<b>14 ± 0,1</b>
FeK	<b>38 ± 0,1</b>	<b>42 ± 1,5</b>
AgL		<b>0,7 ± 0,01</b>

Table 7.4: EDS analysis of SC45 Ag2000 and SC45

The quantitative analysis, in table 7.4, shows a decrease of Na content of 3 % respect to not exchanged glass ceramic and the presence of Ag in atomic percentage of 0,73%. This is in agreement with the ion exchange mechanism, since the sodium ions come out from the glass network (as modifier ions) and are replaced by silver ions, which are present in the molten salt bath. In this case all sodium ions are not replaced by silver one.

## Results and Discussion Antibacterial characterization of SC45

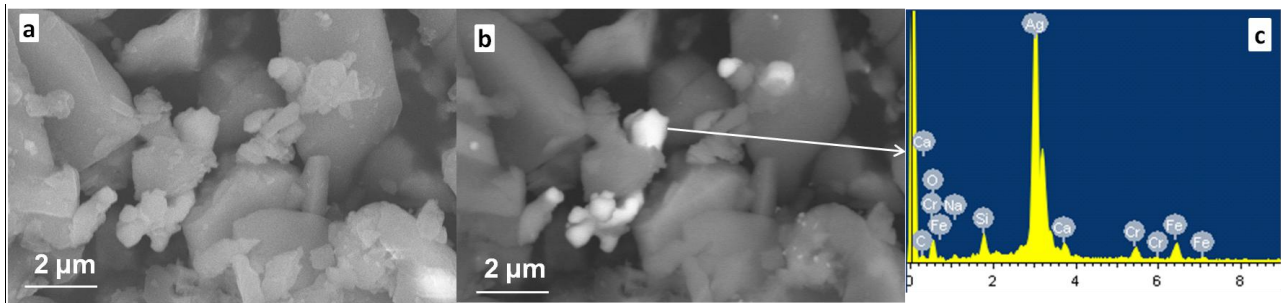


Figure 7.43: Morphology and compositional analysis of SC45 Ag2000

Figure 7.43a reports a secondary electron image and figure 7.43b the same picture in backscattering modality. This modality evidences a contrast between areas with different chemical composition. The image is taken at 30000x . It is clear the presence of silver as confirmed by the EDS analysis performed on one of this particle (figure 7.43c). The peak of silver is the highest of the spectra. The size of the silver particles is sub micrometric and the particle is not completely embedded into the glass matrix.



Figure 7.44: Morphology and compositional analysis of SC45 Ag2000

Figures 7.44a-b represent another analysis performed on SC45 Ag2000 sample in secondary electron and in backscattering modality, respectively. in the black circle a nanoparticle, which could identified as silver, is shown. The EDS analysis reports the silver peak as well as the signals of other elements of glass ceramic composition.

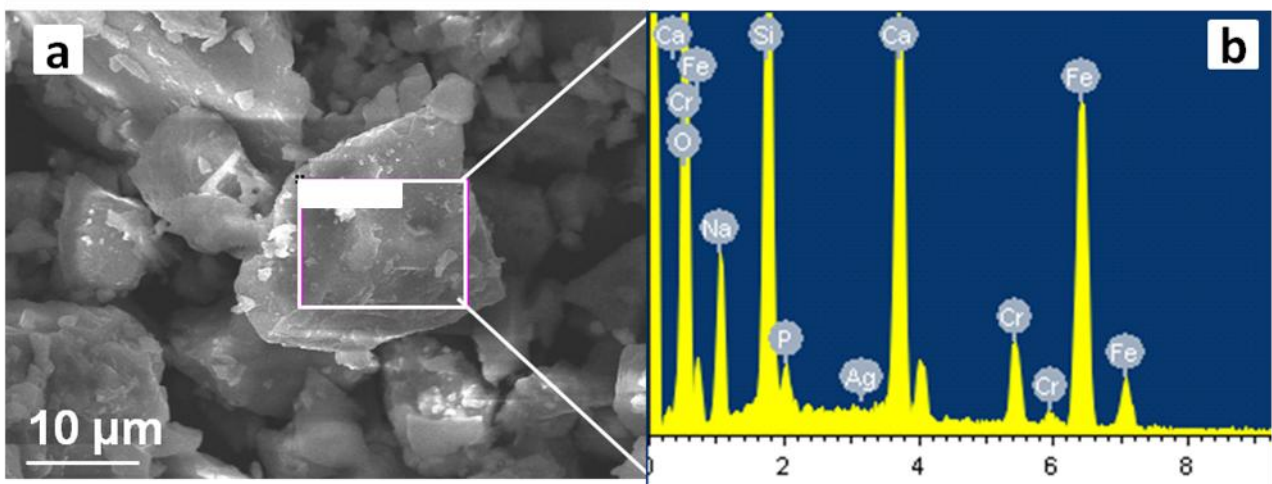


Figure 7.45: Morphology and compositional analysis of SC45 Ag2000

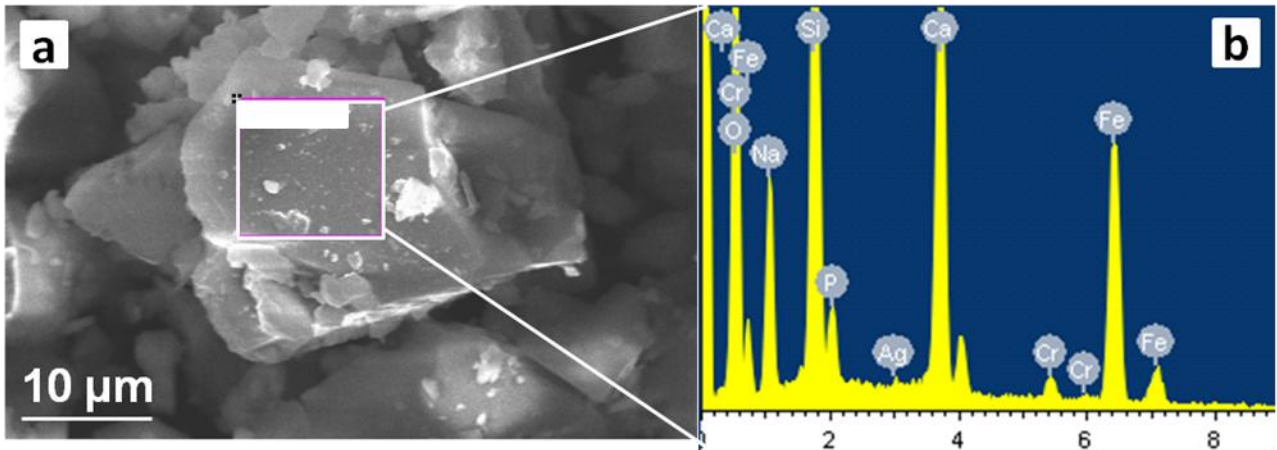


Figure 7.46: Morphology and compositional analysis of SC45 Ag2000

Figure 7.45 a and b report a morphologic and compositional analysis performed on an area of a glass ceramic particle. As it can be seen from the EDS, the peak of silver is lower respect to the other atomic elements. Probably, in this area, silver ion entered into the glass matrix without the formation of micrometric precipitate.

Figure 7.46 a-b report another morphological and compositional analysis of different particle showing the same silver behavior.

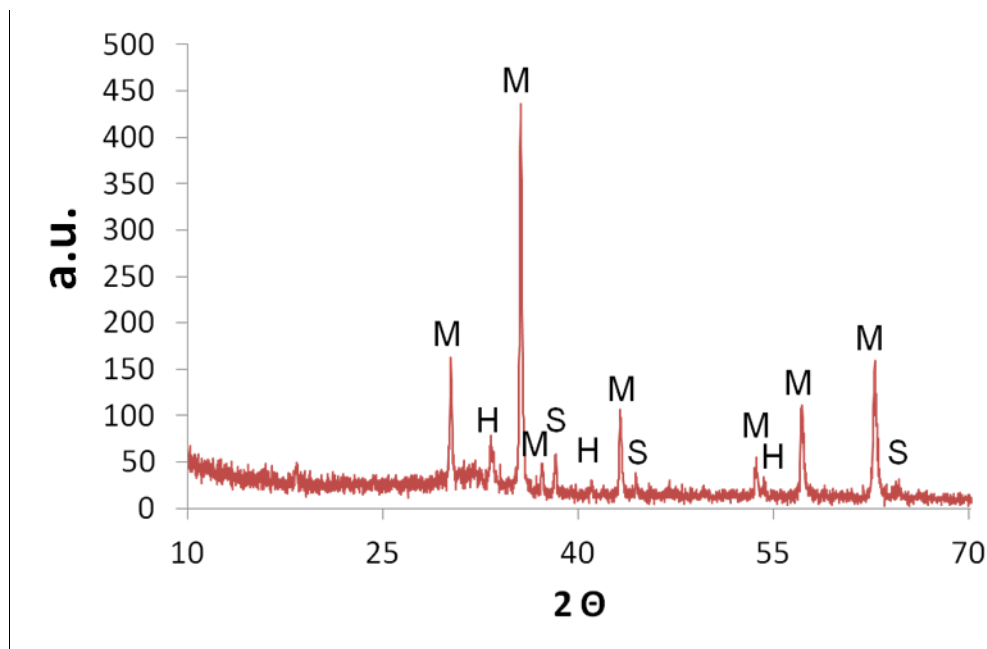


Figure 7.47: X Ray diffraction pattern of SC45 Ag2000

Figure 7.47 presents the XRD investigation shows magnetite as the main crystalline phase into the glass but also metallic silver and small amounts of hematite are present.

In conclusion, with this synthesis method, the silver has been introduced in the glass-ceramic in two different chemical forms: as metallic particles, confirmed by XRD and morphological analysis,

## Results and Discussion Antibacterial characterization of SC45

and as ionic specie, as verified by compositional analysis. The second form is preferred respect to the other because it gains a better antibacterial performance and an effective role in the bacteria membrane interaction. Moreover, the nanoparticles and metallic precipitates of silver included in the glass ceramic matrix permits a prolonged release when it is put in contact with biological fluid. This is preferable because permits a long expression of antibacterial effect .

SC45 Ag2000 in comparison with glass ceramic produced by melting and quenching technique present a smaller metallic silver precipitates. In this case the mean dimension of precipitates are between 1-2  $\mu\text{m}$  respect to those obtained with melting and quenching process which were 10-15  $\mu\text{m}$ . By decrease the dimension of the precipitates the specific surface and so the released silver increase.

### 7.2.10.2. $\text{NaNO}_3:\text{AgNO}_3$ 100:0,5 mol/mol Ag-200

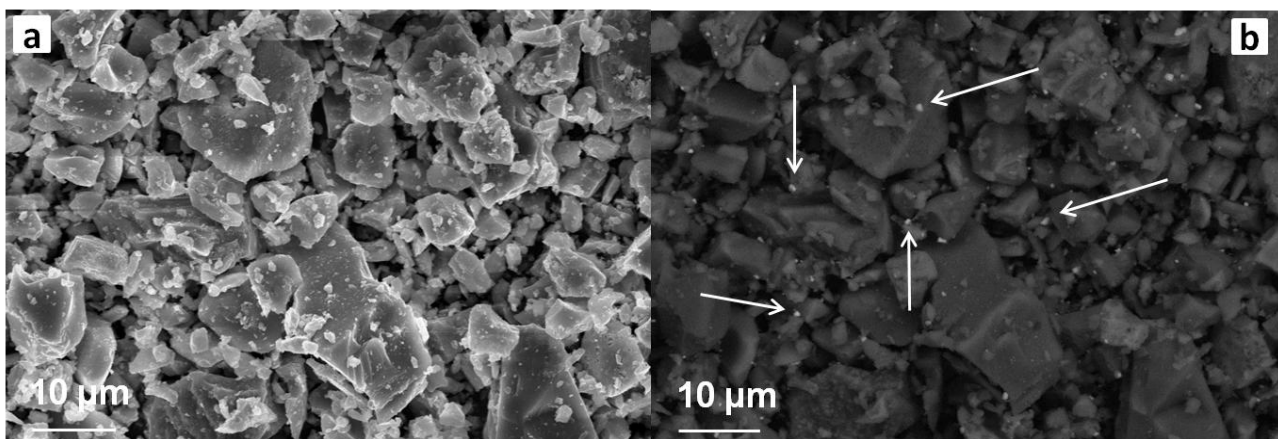


Figure 7.48: Morphology analysis of SC45 Ag200 in secondary electron (a) and backscattering (b)

Figure 7.48a reports the morphology of particles of SC45 after molten salt in ion exchange. The molar concentration of  $\text{NaNO}_3$  and  $\text{AgNO}_3$  is 100:0,5 mol/mol. The silver concentration into the molten salt mix is intermediate among the analyzed ones. In figure 7.48b, acquired with backscattering technique, a large amount of light spots can be seen, as evidenced by the arrows, which can be attributed to silver precipitates.

## Results and Discussion Antibacterial characterization of SC45

	SC45	SC45 Ag200
	%at	%at
NaK	22,5 ± 0,1	16,3 ± 0,09
SiK	21,3 ± 0,2	20,8 ± 0,5
P K	1,6 ± 0,1	1,3 ± 0,09
CaK	16,5 ± 0,1	14,8 ± 0,3
FeK	38 ± 0,1	41,4 ± 0,8
AgL	-	5,4 ± 0,2

Table 7.5: EDS analysis of SC45 Ag200 and SC45

In table 7.5 the atomic percentage of sodium decreases since it is substituted by silver. The introduced silver amount is greater than SC45 Ag 2000. Silica and phosphorus remain constant. Also calcium decreases due to the effect of ion exchange process and iron remains stable.

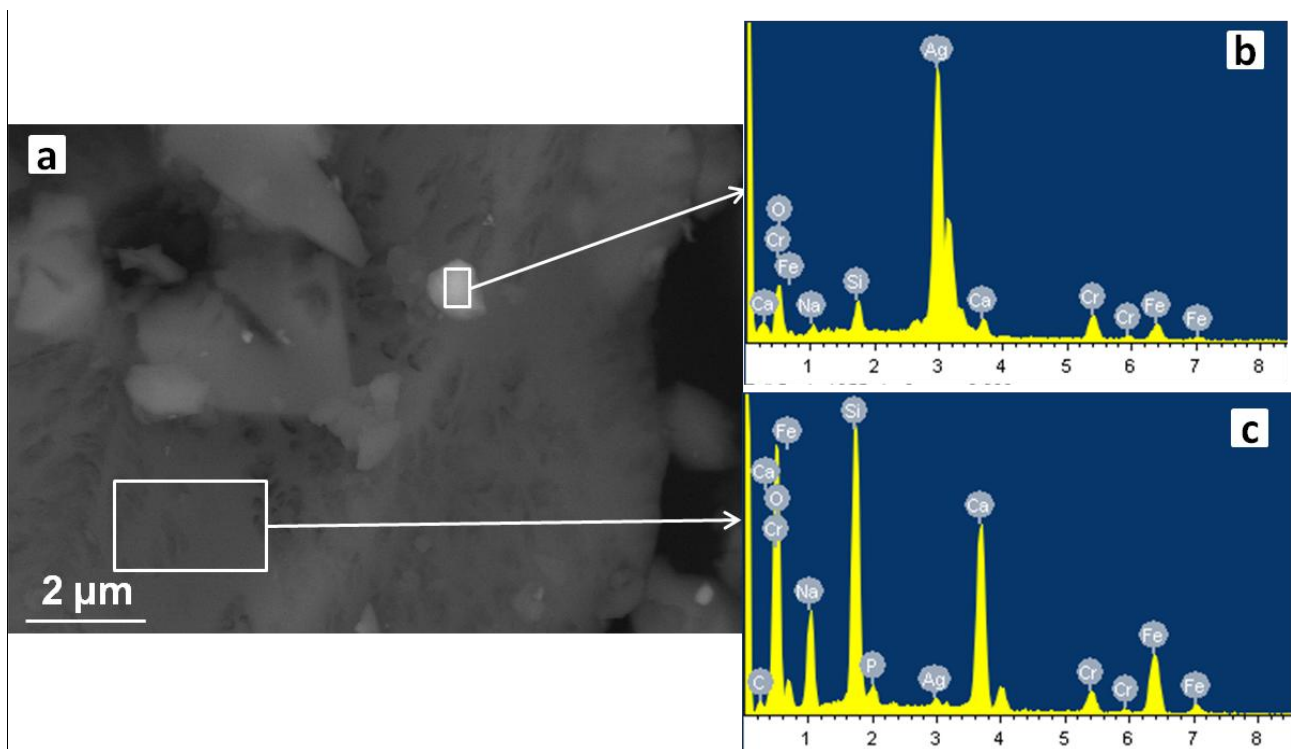


Figure 7.49: Morphology and compositional analysis of SC45 Ag200

Figure 7.49a reports a morphological analysis of a glass particle in which it is possible to distinguish a silver precipitate on the glass-ceramic matrix, as evidenced by the EDS in figure 7.49b (performed on the precipitate) which highlights a peak of silver very sharp and high respect to the peaks of glass elements. On the contrary, figure 7.49c reports a compositional analysis in another part of glass-ceramic, where the peak of silver is not so high as before. It could be assessed that in

## Results and Discussion Antibacterial characterization of SC45

this area silver has been introduced in the glass-ceramic matrix, in small amount, probably in ionic form, by ion exchange.

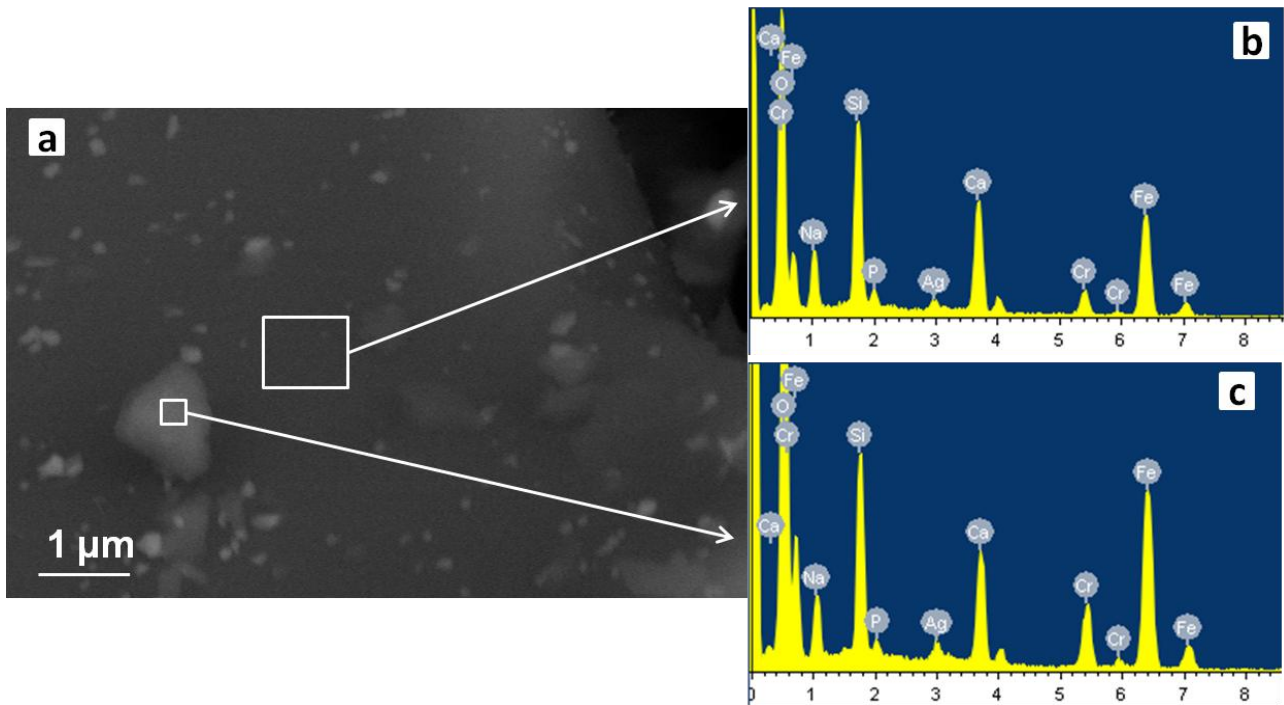


Figure 7.50: Morphology and compositional analysis of SC45 Ag200

Figure 7.50 reports two very similar compositional analyses of different sample surfaces. In figure 7.50b a large area of glass-ceramic is analyzed and in figure 7.50a a smaller one. Spectra are quite similar, they present all peaks characteristic of the glass-ceramic elements and a low silver peak; also in this case it can be hypothesized that the silver is present in ionic form.

In this sample the amount of silver is higher than the amount observed for SC45 Ag2000, so the antibacterial effect will be much evident.

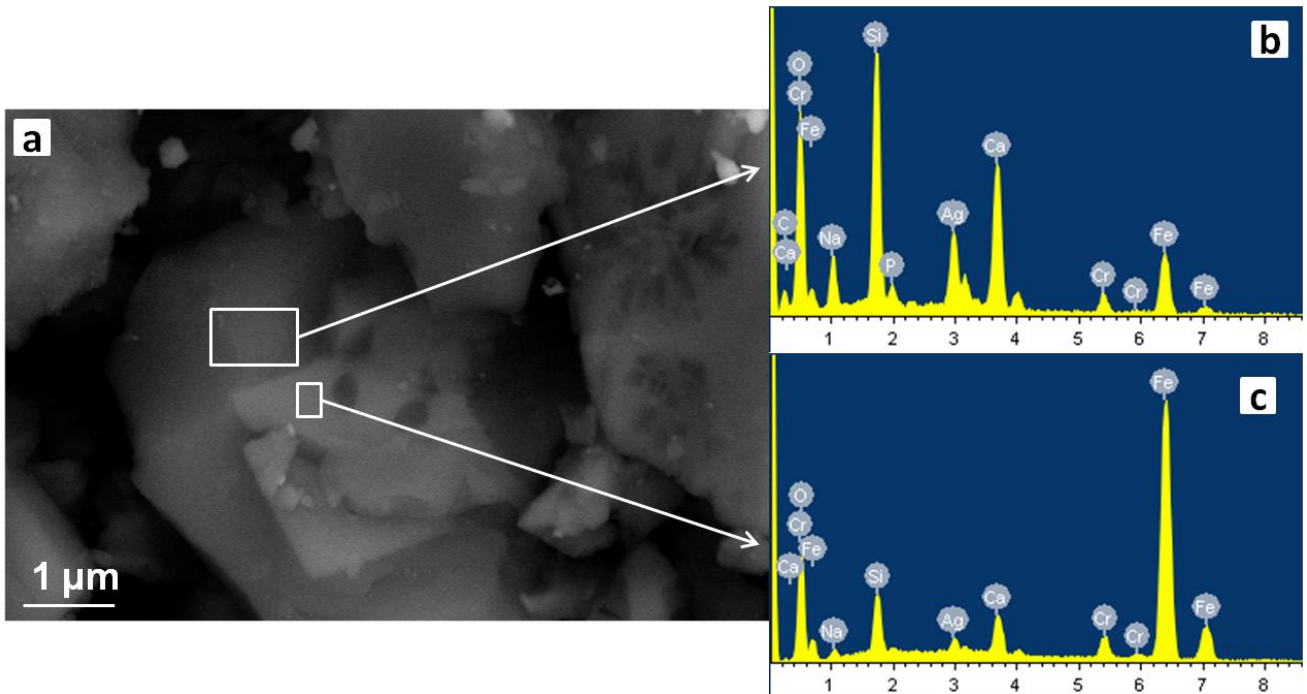


Figure 7.51: Morphology and compositional analysis of SC45 Ag200

Figure 7.51 reports a morphological analysis of a tetrahedral crystal of magnetite embedded into the glass ceramic. The size of columnar crystals is about 3  $\mu\text{m}$  and the glass-ceramic particle about 10  $\mu\text{m}$ . In figure 7.51b EDS spectrum shows the peaks of the SC45 components, with the addition of silver, which probably is in ionic form because, in the morphology, no precipitates are seen. In figure 7.51c the compositional analysis presents a high peak of iron, which confirms the presence of magnetite crystals. The comparison of b and c spectra evidenced that a higher amount of silver is present into the amorphous matrix of the glass-ceramic respect to that detected in the magnetite crystals.

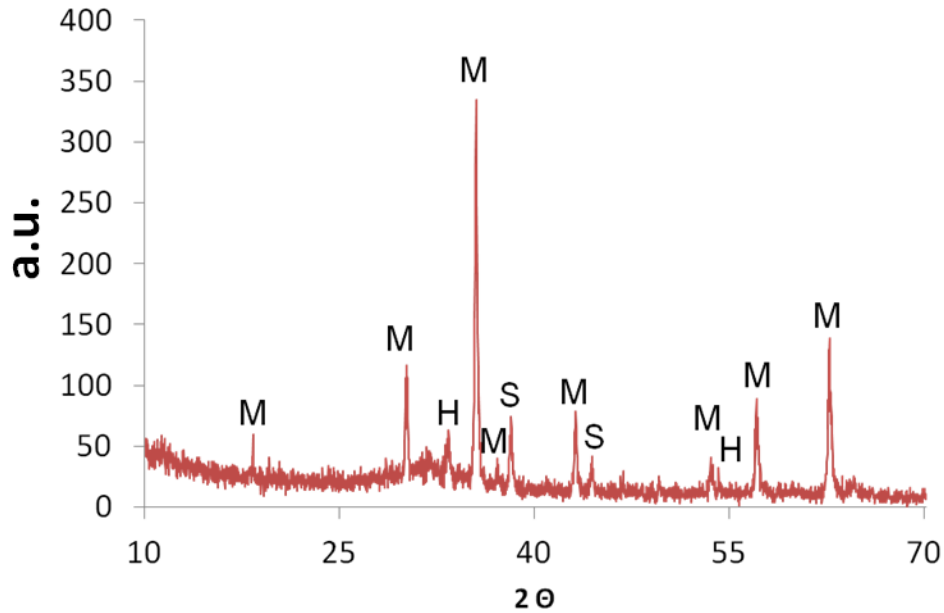
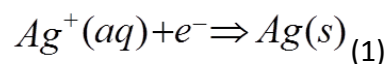


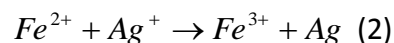
Figure 7.52: XRD pattern of SC45 Ag200

As already assessed by FESEM investigation, the XRD analysis, in figure 7.52, shows magnetite as the main ferrimagnetic phase, together with metallic silver peaks as crystalline phase. The presence of precipitates of metallic silver could negatively affect the reproducibility of the synthesis process. For this reason it should be better to avoid their formation

An hypothesis on the chemical transformation observed on all SC45 doped samples with three different molar concentrations of silver nitrate could be the possibility of an oxidation-reduction reaction between iron and silver. From a theoretical point of view, silver ions in an aqueous solution tend to reduce with the following reaction:



Silver has a higher reduction potential than iron, so it is more inclined to reach a stable metallic form with a consequent oxidation of iron. The chemical reaction developed is:



By increasing the concentration of silver nitrate in the molten an increase of metallic precipitates is observed.

According to the reaction (2), the presence of precipitates may be due to the fact that, in particular for Ag20, the solution was saturated by silver ions and not all of them were able to enter into the glassy network and so they precipitated in these more stable phase such as micro and

nano-particle of metallic silver. Such mechanism occurred in aqueous solution, in the presence of an ion exchange process.

### 7.2.10.3. $\text{NaNO}_3:\text{AgNO}_3$ 100:5 mol/mol Ag-20

This characterization is performed on a sample obtained by ion-exchange in the solution with the highest amount of silver concentration into the molten salt.

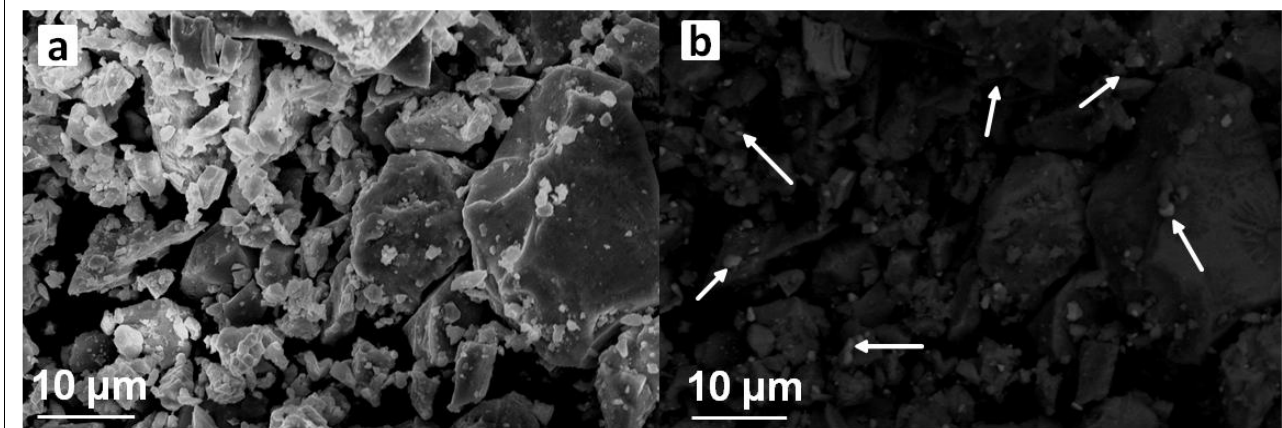


Figure 7.53: Morphology analysis of SC45 Ag200 sample in secondary electron (a) and backscattering (b).

Figure 7.53 reports secondary electron image (a) and backscattering (b) of the particles  $< 20 \mu\text{m}$  of SC45 after the exchange in the solution 100: 5 mol/mol. Also in this case it was observed the presence of different precipitates as indicated by white arrows.

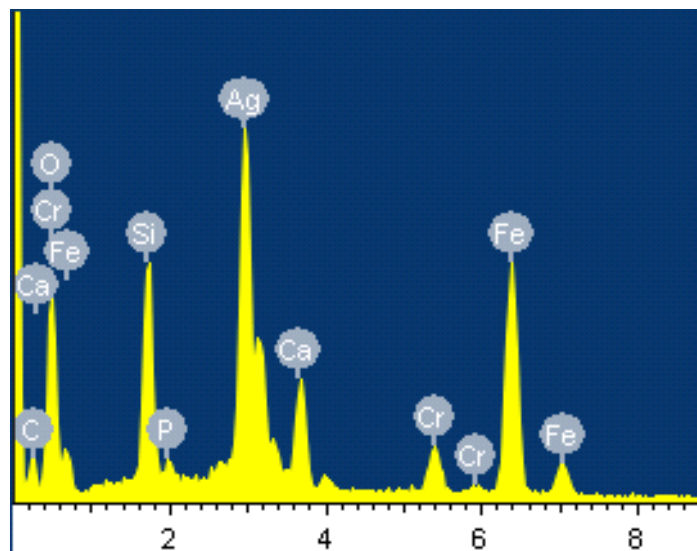


Figure 7.54: Compositional analysis of SC45 Ag20 sample

The compositional analysis, in figure 7.54, presents a high peak of silver together with the other chemical components of the glass ceramic.

## Results and Discussion Antibacterial characterization of SC45

	SC45	SC45 Ag20
	%at	%at
NaK	22,5 ± 0,1	1,8 ± 0,2
SiK	21,3 ± 0,2	20,4 ± 0,4
P K	1,6 ± 0,1	1,4 ± 0,2
CaK	16,4 ± 0,15	12,3 ± 0,40
FeK	38,01 ± 0,1	40,5 ± 0,8
AgL		23,5 ± 0,6

Table 7.6: EDS analysis of SC45 Ag20 and SC45

The EDS compositional analysis in figure 7.6 evidences a very high depletion of sodium and a clearly decrease of calcium, a light increase of iron and the introduction of 23,5 %at of silver into the glass-ceramic. The ionic exchange involved mainly sodium and silver. This depends on the fact that silver ions possess an atomic ratio likes of sodium. Moreover, it was proved that silver ions are able to take part to the bioactivity mechanism with the same function of sodium[5]: when the release of silver ion occurs the non-bridging oxygen create the condition for the silica gel formation, which is the first step for the precipitation of hydroxyapatite on a bioactive glass surface [6].

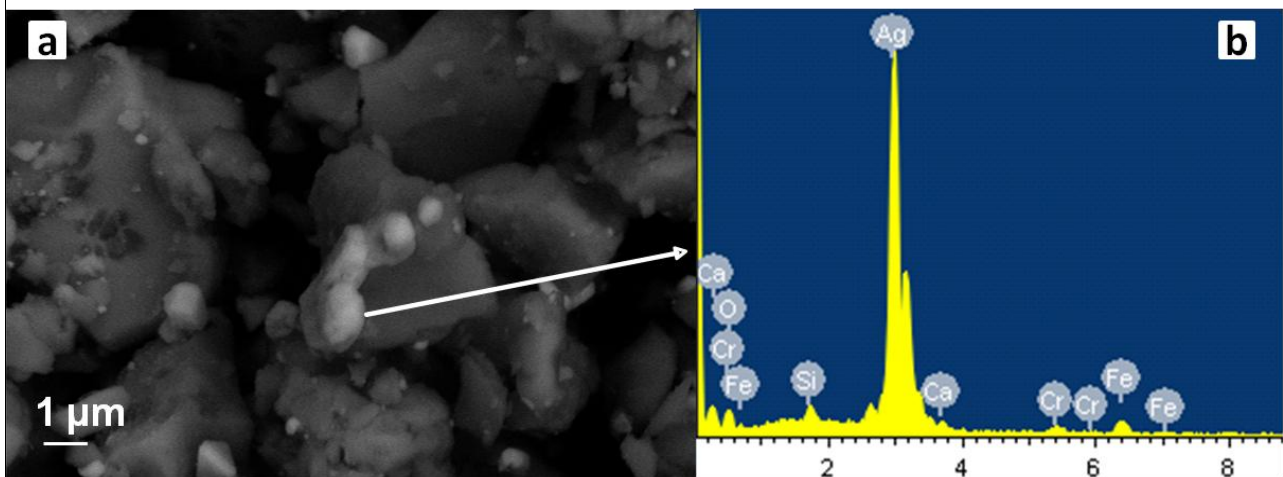


Figure 7.55: Morphology and compositional analysis of SC45 Ag20

Figure 7.55 a-b reports a morphological and compositional analysis on SC45 Ag20. The EDS analysis performed on a bright precipitate evidences a strong peak of Ag. The image was recorded in backscattering modality for a better visualization of precipitates.

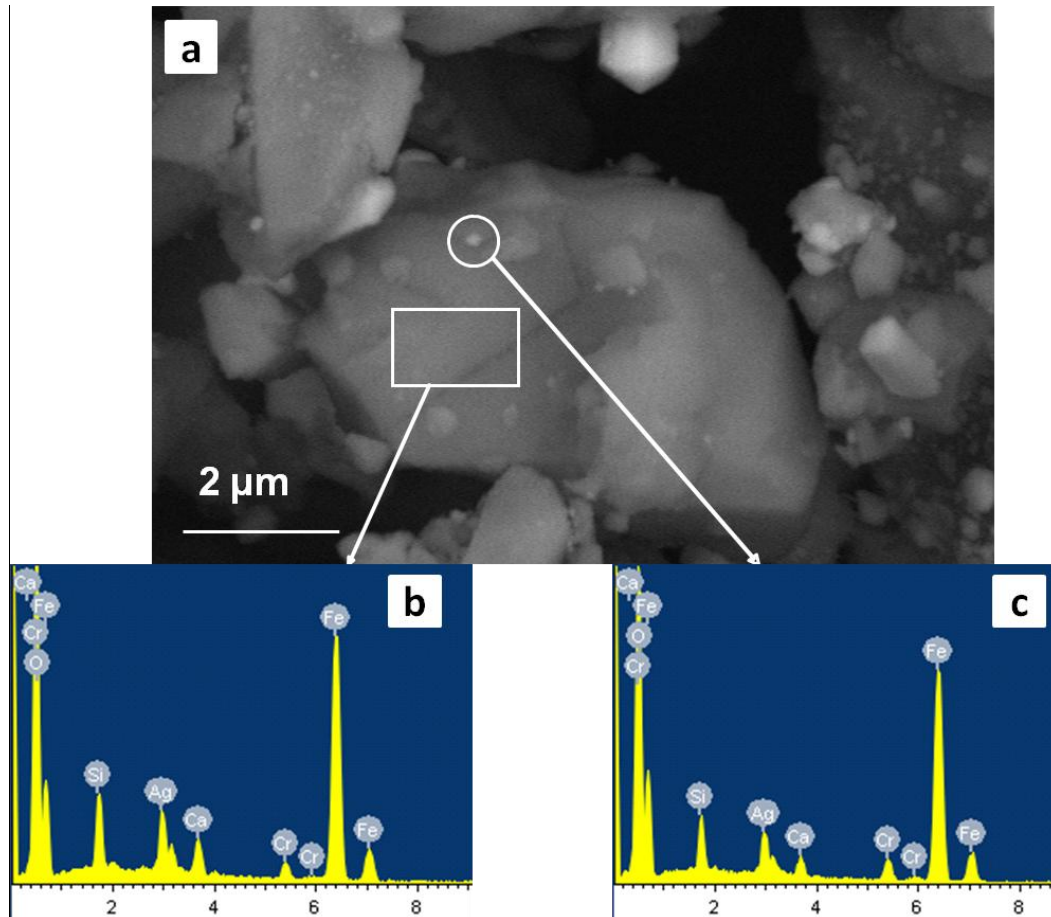


Figure 7.56: Morphology and compositional analysis of SC45 Ag20

This figure 7.56a shows a glass ceramic particle on which two different EDS analyses have been performed. Figure 7.55b presents all the peaks of SC45 with silver, that it is likely to be entered in the glass matrix in ionic form, since any bright particles are visible into the area on which the analysis was performed. Figure 7.56c highlights the presence of a silver nanoparticle. This is important because the nanometric size of silver has a positive effect as antibacterial: first of all nanometric particles expose a wide specific surface area than micrometric ones and so they can release a greater amount of silver; moreover silver nanoparticles possess an antibacterial mechanism different from ionic silver

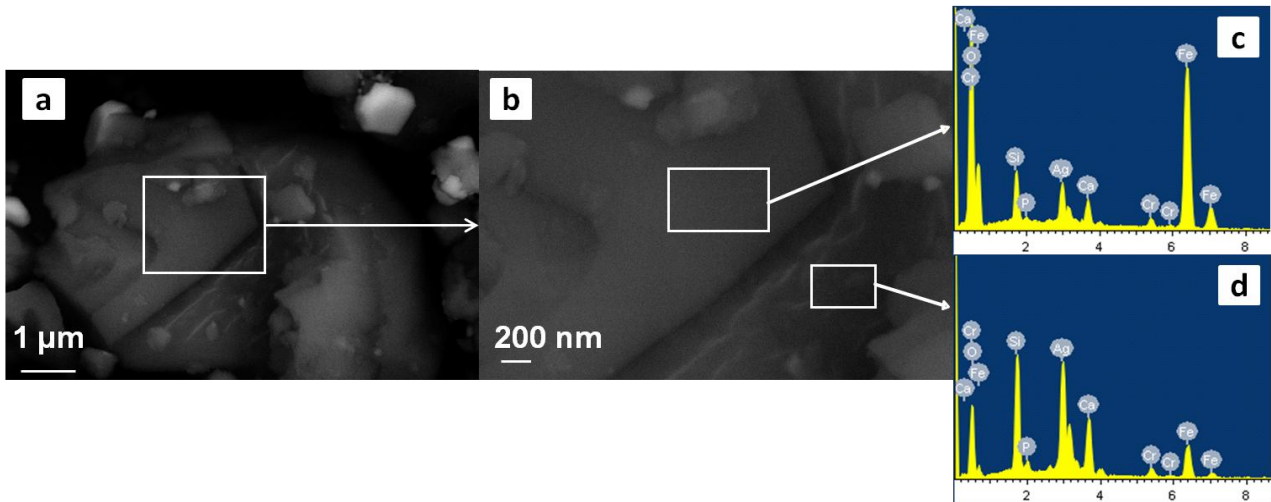


Figure 7.57: Morphology and compositional analysis of SC45 Ag20

Figure 7.57a reports a magnification of magnetite crystal included in the glass ceramic matrix. Figure 7.57b evidences a magnification where two compositional analyses are performed on different areas of sample surfaces. Silver seems to be entered both on the ceramic phase as confirmed by EDS in figure 6.57c and in the vitreous network as confirmed by EDS in figure 7.57d. EDS in figure 7.57c presents a high peak of iron because the analysis is performed on a magnetite crystal, while in EDS analysis of figure 5.57d a high peak of silicon is detected, together with the other glass ceramic elements, since the analysis is realized on the amorphous matrix.

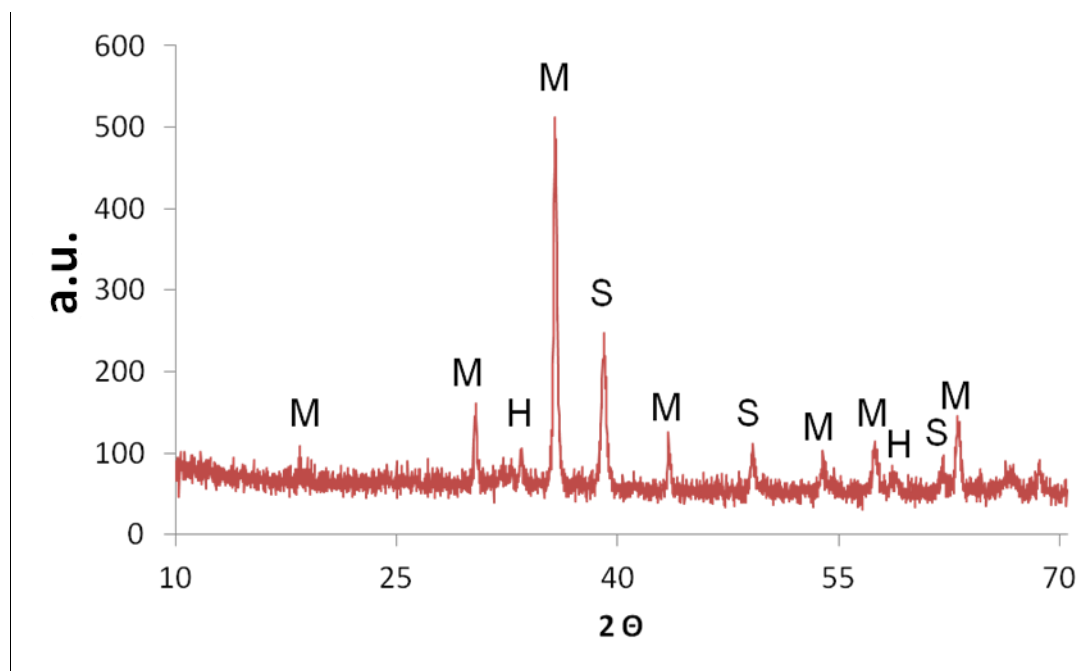


Figure 7.58: XRD pattern of SC45 Ag20

Figure 7.58 reports the X-ray analysis performed on SC45 Ag20 shows magnetite as the main crystal phase and very intense and narrow peaks metallic silver is also detected. Traces of

hematite are always present. At low diffraction angles between 20-35 °  $\Theta$  there is a halo, typical of amorphous phase.

#### 7.2.10.4. $\text{NaNO}_3:\text{Cu}(\text{NO}_3)_2$ 100:0,05 mol/mol Cu-2000

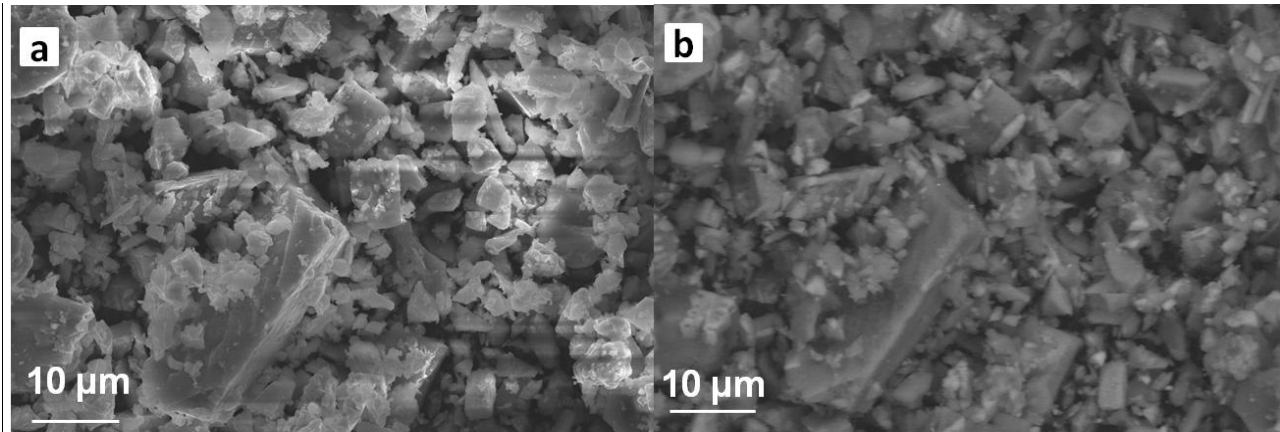


Figure 7.59 : Morphology analysis of SC45 Cu2000

Figure 7.59a reports a secondary electron image, acquired in secondary electrons, which gives an overview of the morphology of SC45 sample treated with the ion exchange process in molten salts (SC45 Cu 2000) and in figure 7.59b the same image in backscattering shows the different phases of the material. No copper precipitates, both as micro and nano particle, can be seen.

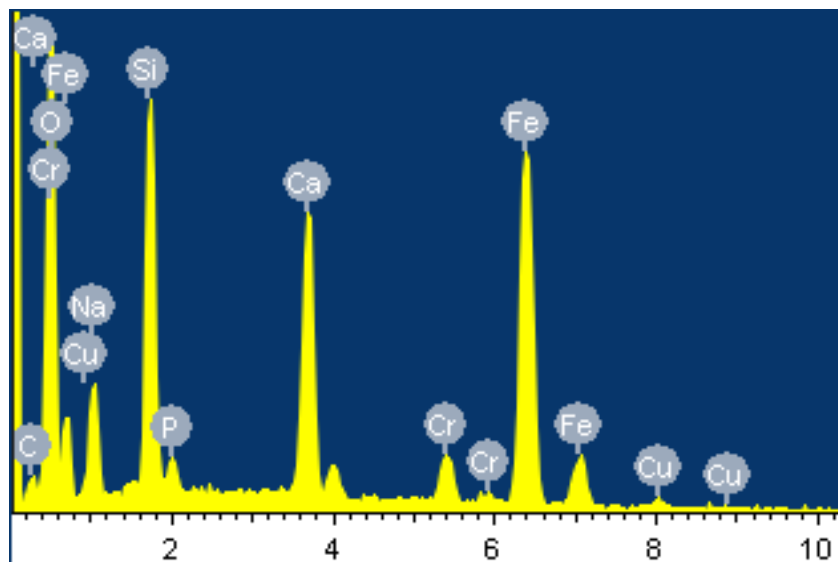


Figure 7.60: Area Compositional analysis of SC45 Cu2000

The compositional area analysis shows the peaks of the glass-ceramic characteristic components, as oxygen, sodium, calcium, phosphorus, silicon and iron; chromium is not part of the glass-ceramic but was applied on its surface for scanning microscopy observation. After the ion exchange treatment, copper is present in the composition of the glass ceramic.

## Results and Discussion Antibacterial characterization of SC45

	SC45	SC45-Cu2000
	%at	% at
NaK	22,5 ± 0,1	19,1 ± 0,1
SiK	21,3 ± 0,22	20,9 ± 0,4
P K	1,6 ± 0,12	1,3 ± 0,1
CaK	16,5 ± 0,15	15,1 ± 0,3
FeK	38 ± 0,1	41,3 ± 0,6
CuK		2 ± 0,3

Table 7.7: EDS analysis of SC45 Cu 2000 respect to SC45.

Table 7.7 reports the EDS area analysis results of SC45 Cu2000 and of the untreated SC45. The analysis of area shows a decrease of Na with an introduction of Cu quantity at 2% .

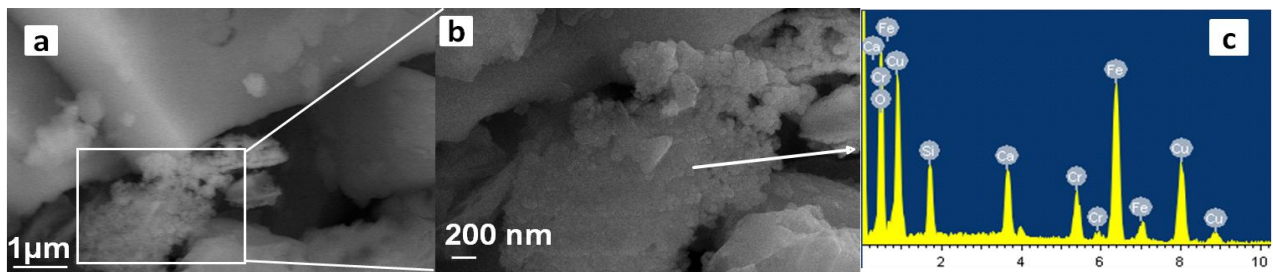


Figure 7.61: Morphology and compositional analysis of SC45 Cu2000

In figure 7.61a-b-c, the presence of some very small agglomerated particles with different morphology respect to glass-ceramic are evidenced; through the EDS analysis, made on such agglomerated, shown in figure 7.61c, it can be seen that the concentration of copper is particularly high. These particles don't present the morphology of metallic copper, they probably are traces of copper salts precipitated on the material surface during the ion exchange. Copper may have more tendency to form salts rather than entering as ion into the silica network.

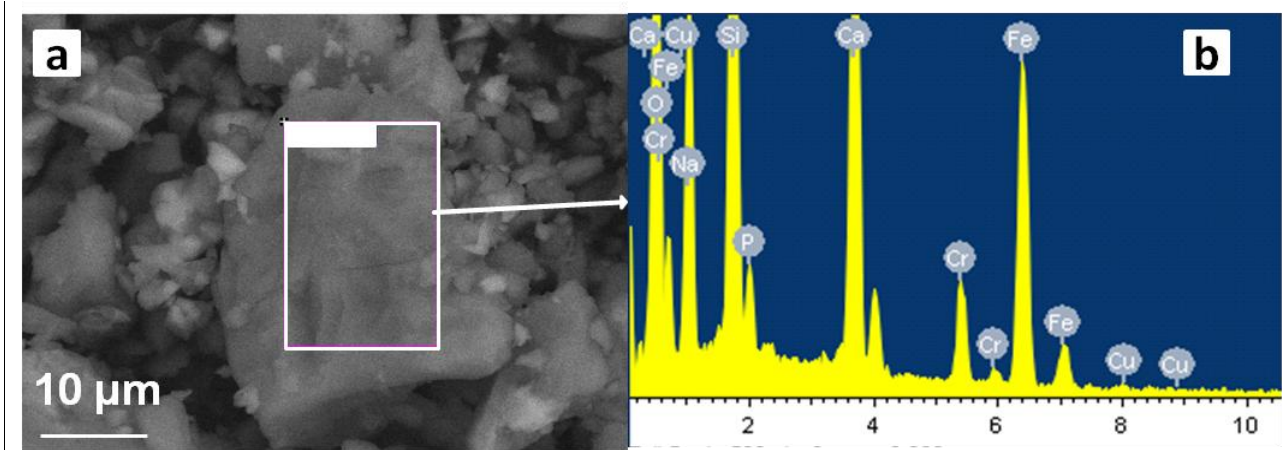


Figure 7.62: Morphology and compositional analysis of SC45 Cu2000

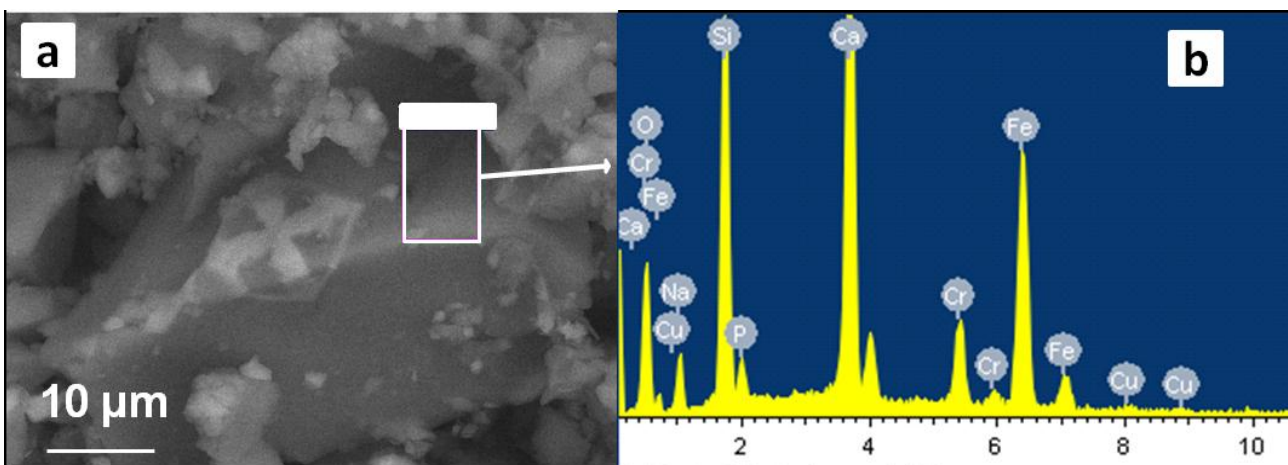


Figure 7.63: Morphology and compositional analysis of SC45 Cu2000

To verify the effective presence of copper within the amorphous glass ceramic matrix, EDS analysis was performed. Different glass ceramic zones (see figures 7.62a-b 7.63a-b), apparently free from magnetite crystals or other smaller particles were analyzed. The performed analysis shows a small content of Cu in the SC45 particles. The proportion of copper present within the glass-ceramic is low compared to other components such as silicon, iron, sodium, calcium and phosphorus.

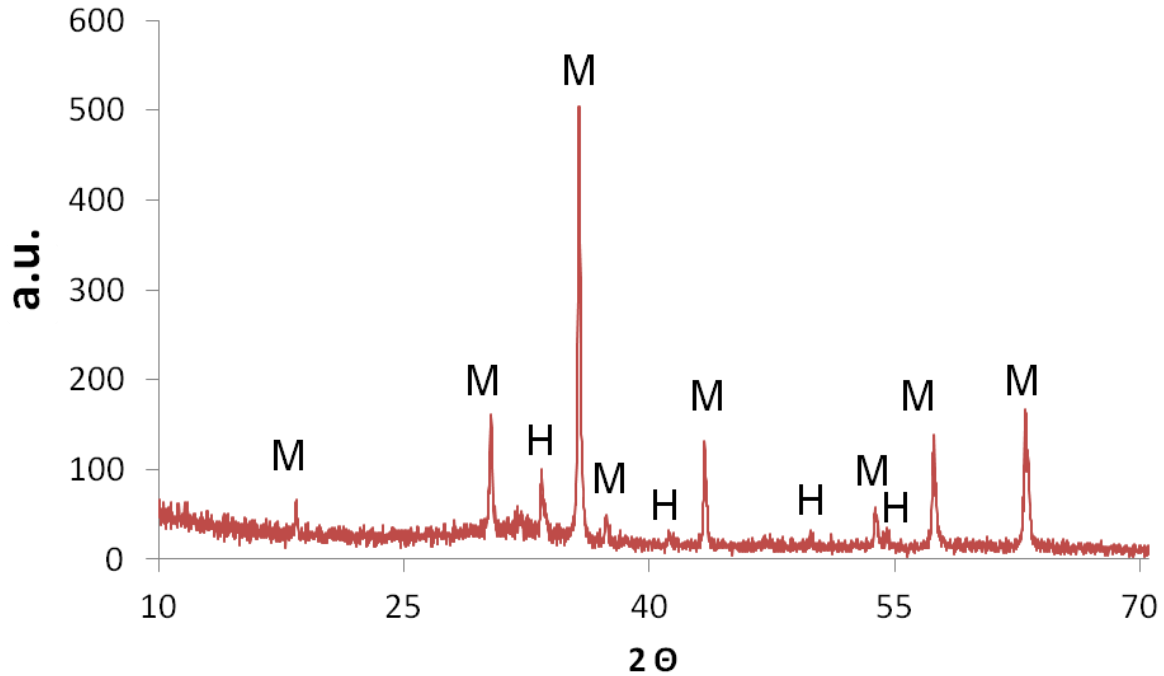


Figure 7.64: XRD analysis of SC45 Cu2000

Figure 7.64 reports XRD pattern of SC45 doped with a molar ratio of  $\text{NaNO}_3/\text{Cu}(\text{NO}_3)_2$  equal to 2000 does not show any metallic copper or any crystalline phase containing copper. The main phase of the pattern is magnetite, and a low amount of hematite is also present. Probably the presence of some precipitates, visualized in the FESEM images, is too low to be detected by XRD.

#### 7.2.10.5. $\text{NaNO}_3:\text{Cu}(\text{NO}_3)_2$ 100:0,5 mol/mol Cu-200

The images in figure 6.65 show the morphology of the sample at low magnification in the secondary electrons in (a) and backscattering (b) respectively.

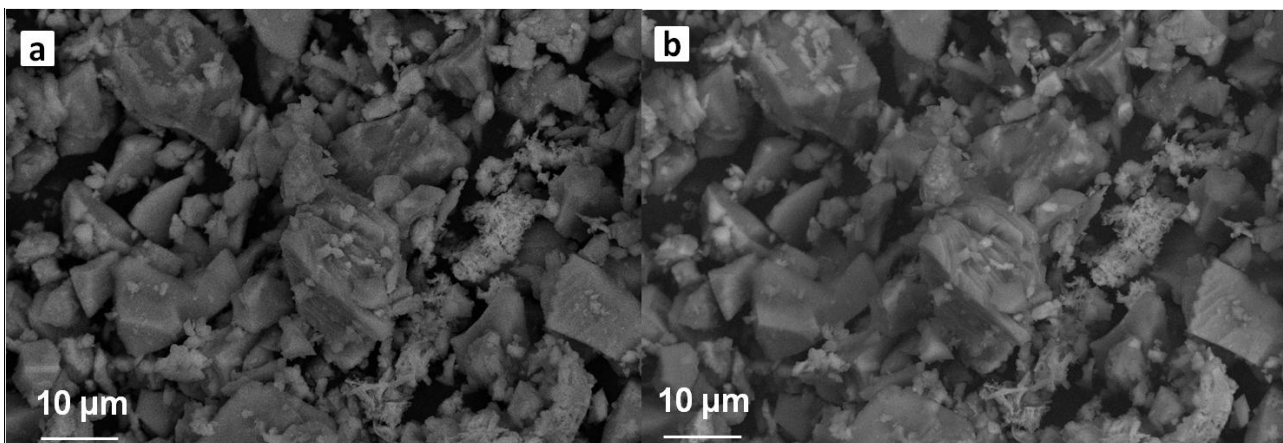


Figure 7.65: Morphology and compositional analysis of SC45 Cu200

## Results and Discussion Antibacterial characterization of SC45

	SC45	SC45-Cu200
	%at	%at
NaK	22,5 ± 0,1	12,2± 0,1
SiK	21,3 ± 0,2	21,3±0,2
P K	1,6 ± 0,1	1,5±0,1
CaK	16,5 ± 0,1	14,8±0,2
FeK	38 ± 0,1	45,1±0,1
CuK		5,1±0,3

Table 7.8: EDS analysis of SC45 Cu 200 respect to SC45.

The EDS compositional analysis of SC45 Cu200 shows an increase of copper concentration respect to SC45 Cu2000. Sodium decrease of 45% respect to the SC45 .

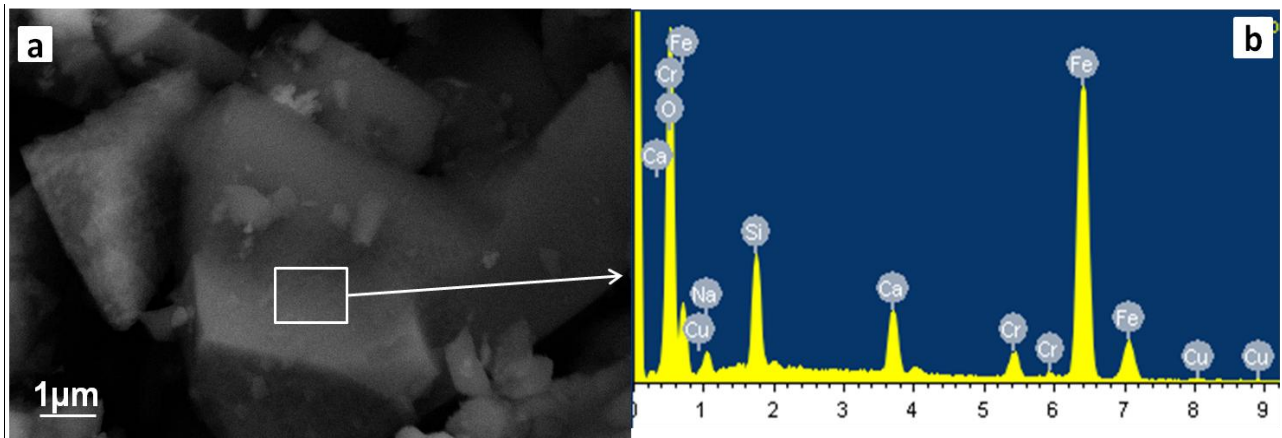


Figure 7.66: Morphology (a) and compositional analysis (b) of SC45 Cu200

Figure 7.66a presents the morphology of a particle on which a compositional analysis was performed. Copper is not visible as metallic precipitate, so it seems to be present, in small amount, in ionic form into the glass ceramic network.

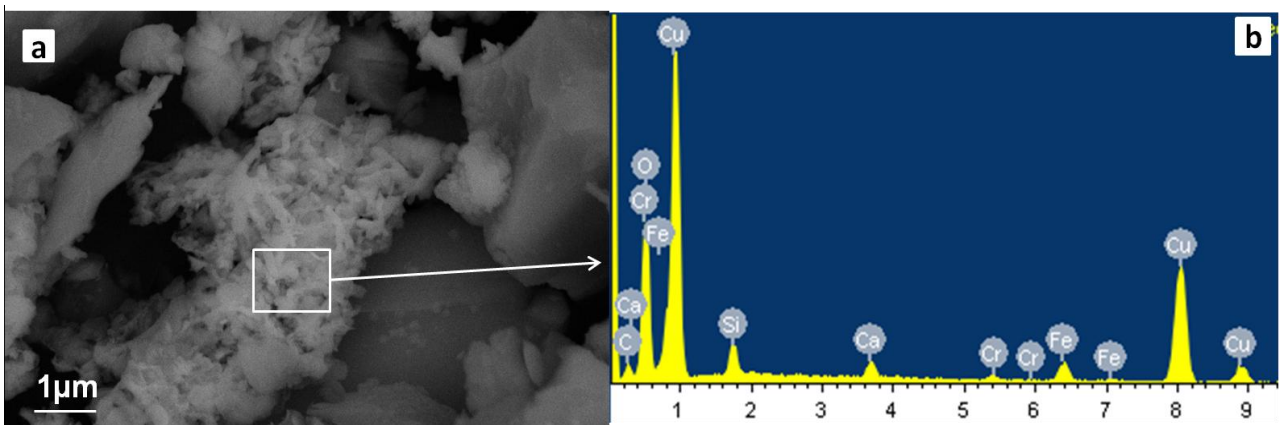


Figure 7.67: Morphology (a) and compositional analysis (b) of SC45 Cu200

## Results and Discussion Antibacterial characterization of SC45

Figure 7.67a reports the morphology of a copper-rich precipitate. As it can be seen from the picture the morphology is different from the glass particle. Even the EDS analysis presents high peaks of copper and oxygen. During the synthesis process, probably a part of copper produced a copper oxide.

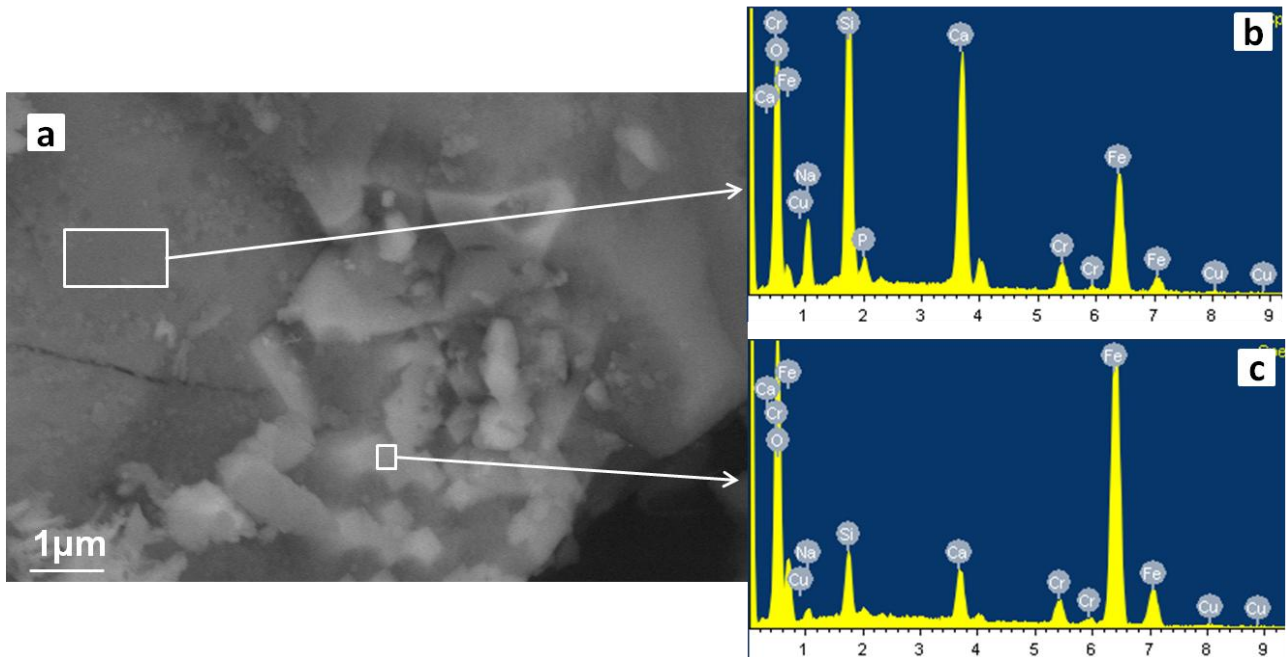


Figure 7.68: Morphology and compositional analysis of SC45 Cu200

Image 7.68 reports a morphological overview of a glass particle with magnetite crystals included into the glass ceramic. Probably the compositional analysis performed on two different points of the particle (see arrows) evidences the presence of copper both in the glass matrix and in the magnetite crystal. This is an hypothesis because the beam penetrates up to about 1 microns in the analyzed surface and, if the analyzed crystal is thinner, it can detect also elements belonging to the amorphous phase.

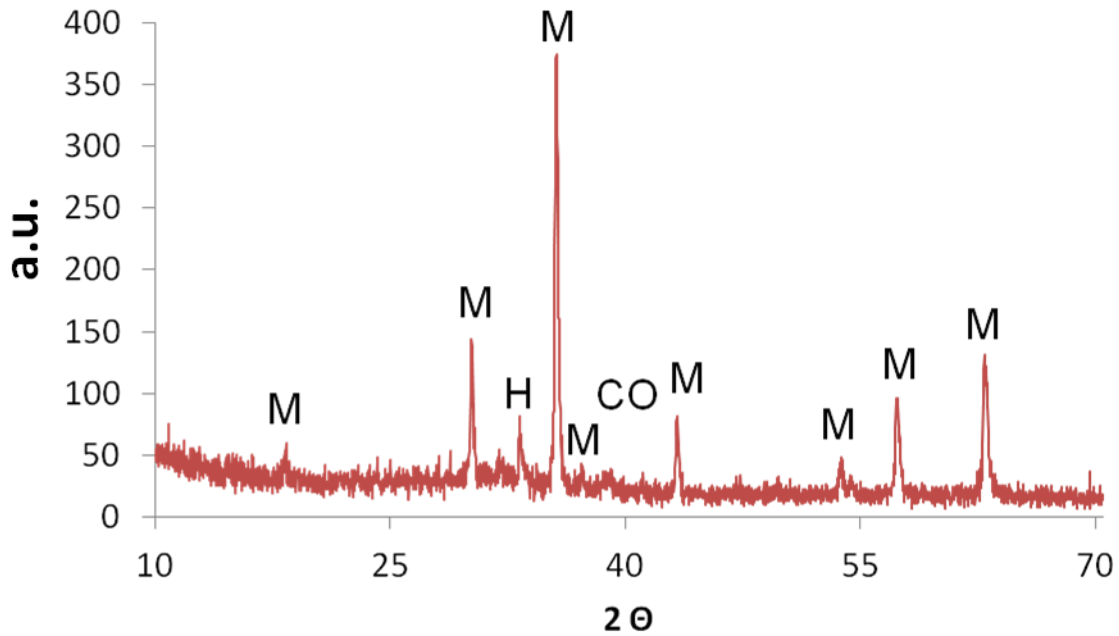


Figure 7.69: XRD pattern of SC45 Cu200 . Magnetite (M) , Hematite (H) and trace of copper oxide (CO)are detected

XRD analysis is in agreement with the FESEM characterization, magnetite is the main magnetic crystalline phase with a negligible amount of hematite. Copper oxide is present, with a low peak, in agreement with figure 7.69.

#### 7.2.10.6. NaNO<sub>3</sub>:Cu(NO<sub>3</sub>)<sub>2</sub> 100:5 mol/mol Cu-20

The following FESEM, EDS and XRD analyses were performed on the samples with the highest copper molar concentration.

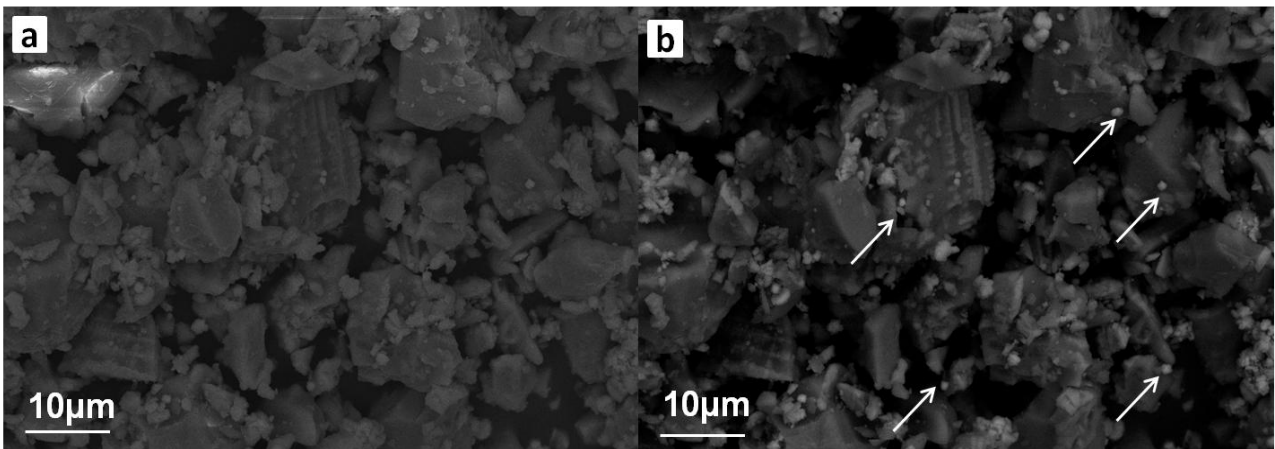


Figure 7.70: Morphology analysis in InLens modality (a) and backscattering (b) of SC45 Cu 20 samples

## Results and Discussion Antibacterial characterization of SC45

Figure 7.70 reports the secondary electron image (a) and backscattering (b) of SC45 particles (<20  $\mu\text{m}$ ) after the ion exchange (Cu 20). It can be observed the presence of some diffuse precipitates among the glass particles (see with arrows).

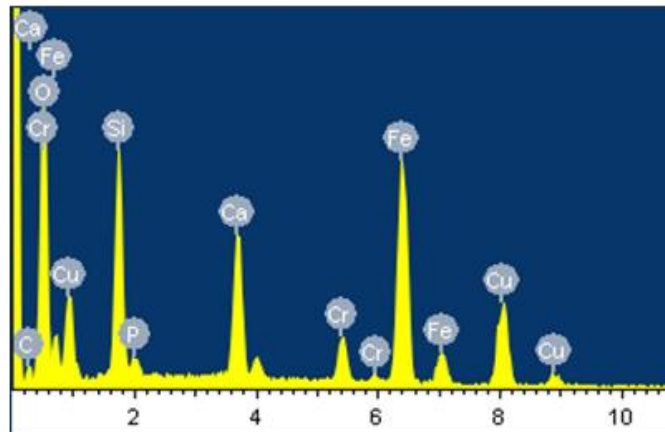


Figure 7.71: Area compositional analysis of Sc45 Cu20

EDS analysis in figure 7.71 shows how the concentration of copper is greatly increased if compared to the first experiment with SC45 Cu2000. The other peaks are characteristic of the glass ceramic, except for chromium, which come out from the metallization process for the FESEM analysis.

	SC45	SC45-Cu20
	%at	%at
NaK	22,5 $\pm$ 0,1	0,7 $\pm$ 1,2
SiK	21,3 $\pm$ 0,2	14,5 $\pm$ 0,9
P K	1,6 $\pm$ 0,1	1,1 $\pm$ 0,1
CaK	16,4 $\pm$ 0,1	6,2 $\pm$ 0,6
FeK	38 $\pm$ 0,1	17,3 $\pm$ 3
CuK		60 $\pm$ 4,2

Table 7.9: EDS analysis of SC45 Cu20 respect to SC45

In table 7.9 the area EDS analysis shows almost total depletion of sodium, a decrease of 10,3% of calcium and the introduction of a 60% of copper. All sodium ions were released by the glass matrix and a part of them has replaced by copper ions, while another quantity is precipitated as copper oxide. Probably copper substitutes even calcium sites in the network, even if the calcium ion

## Results and Discussion Antibacterial characterization of SC45

mobility is much lower respect to the sodium one[3]. Also the amount of iron and silica present a large variation

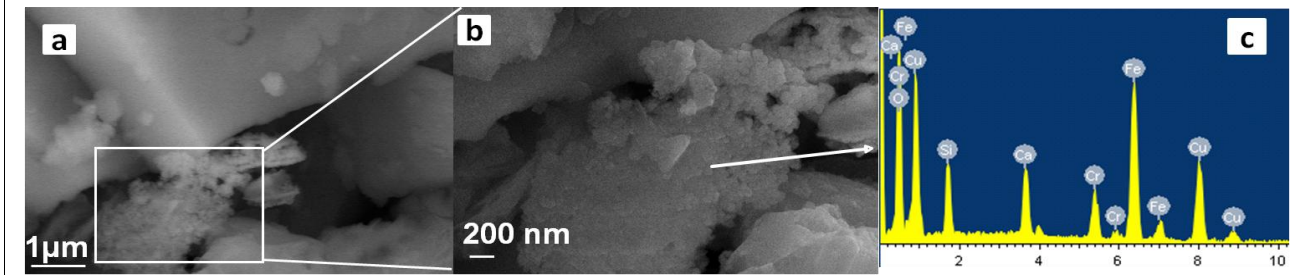


Figure 7.72: Morphology (a-b) and compositional (c) analysis of SC45 Cu20

Figure 7.72a shows some particles with different morphology respect to the SC45 particles. The backscattering analysis in figure 7.72b evidences as the presence of large agglomerates, which can be attributed to copper precipitates (see also the high Cu peaks present in the EDS analysis in figure 7.72c). Analysis on the precipitates shows the presence of a high quantity of copper and oxygen.

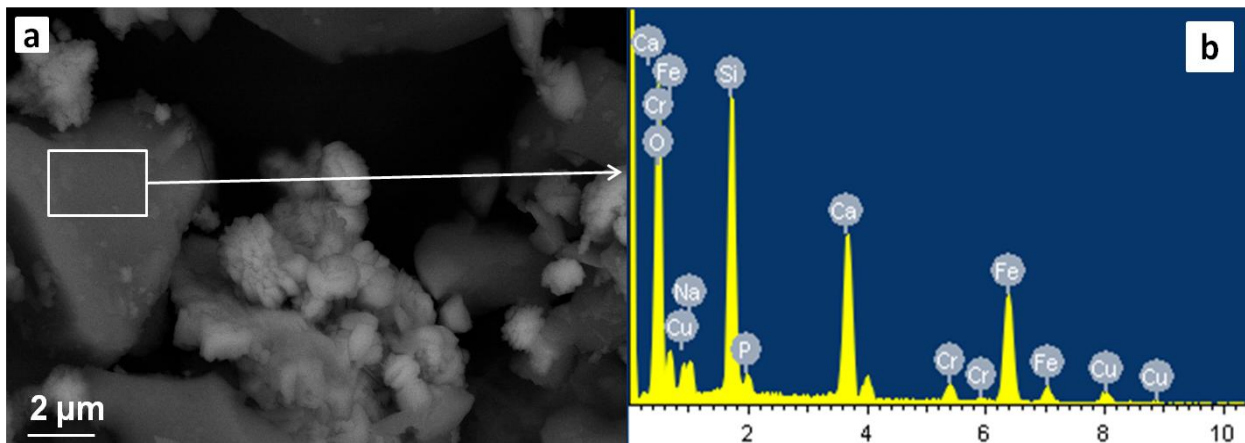


Figure 7.73: Morphological and compositional analysis of SC45 Cu20

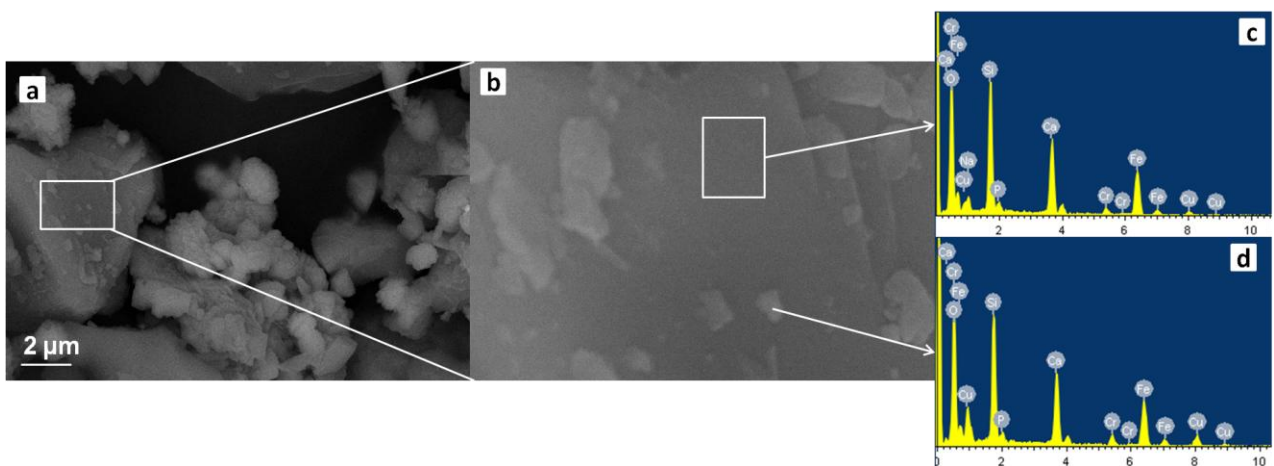


Figure 7.74: Morphological and compositional analysis of SC45 Cu20

## Results and Discussion Antibacterial characterization of SC45

Figure 7.74a reports a morphological characterization of the glass ceramic particles nearby the copper precipitate. EDS in figures 7.74b and 7.74c performed on the SC45 Cu20 surface, shows a greater amount of copper in comparison to Cu2000. Moreover, sodium is also present. As evidenced by the corresponding morphology, the surface is apparently free from precipitates. Figure 7.74b presents a morphological surface magnification of the figure 7.74a where two EDS analyses have been in different points. EDS in figures 7.74c and 7.74d evidence that copper is present both in the small glass ceramic particles and not only in the matrix. Copper precipitates as an oxide but it is also present in the glass ceramic powder in a little amount.

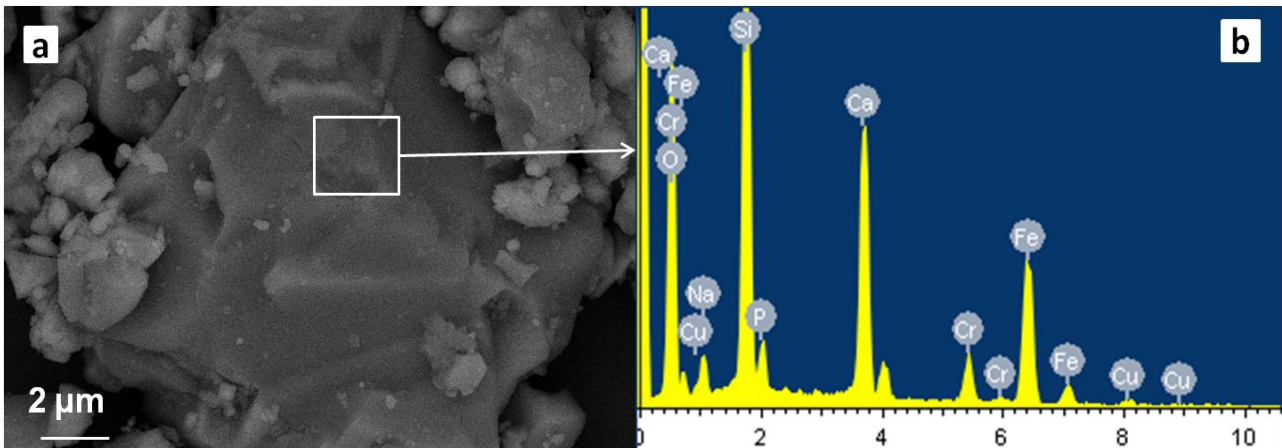


Figure 7.75: Morphological (a–b) and compositional (c–d–e) analysis of SC45 Cu20

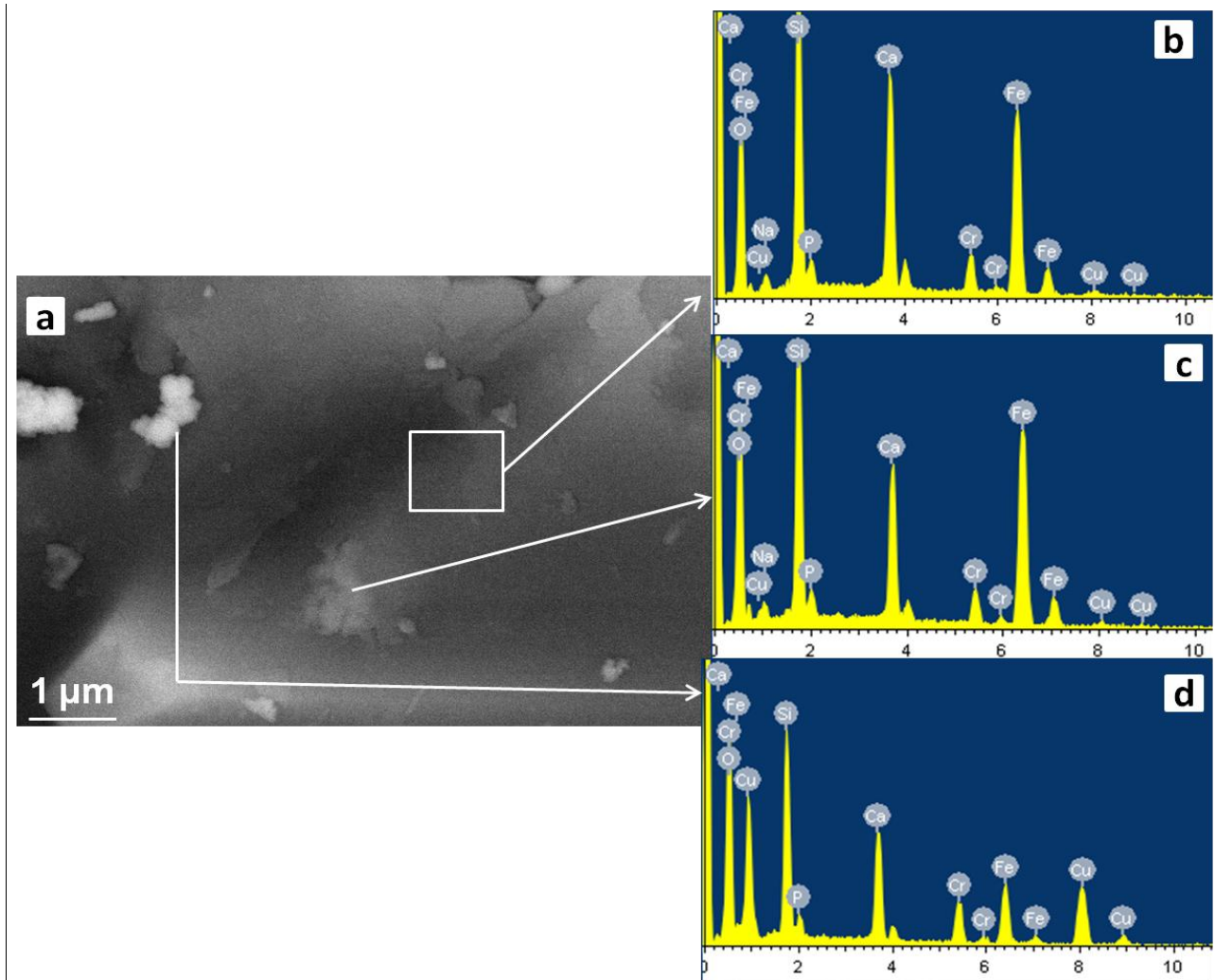


Figure 7.76: Morphological (a –b) and compositional (c-d-e) analysis of SC45 Cu20

Figure 7.76a reports a surface magnification of a large SC45 particle and EDS in figure 7.75b-c-d demonstrates how the copper is penetrated into the glass ceramic. After the magnification of the central part of the particle surface (figure 7.76b), EDS was performed in different points of the figure 7.76a. The analysis performed on a probable precipitate evidences a higher copper peak.

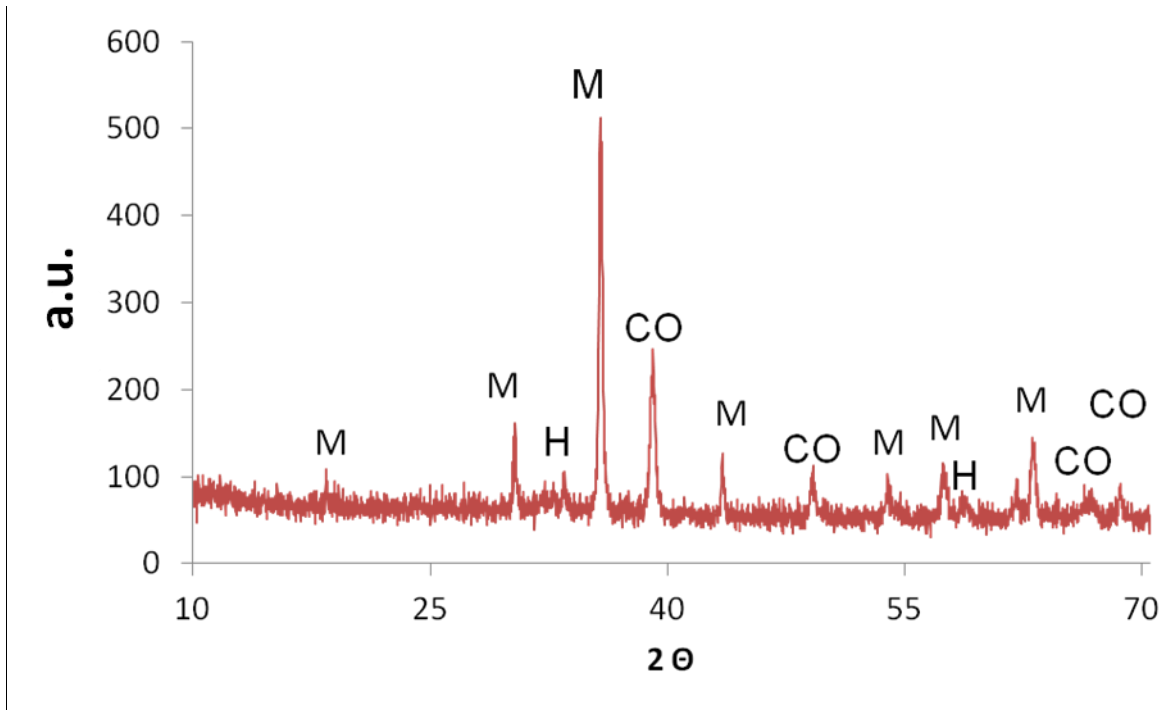


Figure 7.77: XRD pattern of SC45 Cu<sub>20</sub>. Magnetite (M) , hematite (H) and copper oxide (CO) is detected.

X-ray analysis performed on a sample of SC45 Cu<sub>20</sub> is shown in Figure 7.77. The presence of magnetite and hematite, as in the previous cases, is reported. A significant difference respect SC45 Cu<sub>2000</sub> and SC45 Cu<sub>200</sub> spectra is given by the high concentration of copper oxide, because the concentration of the copper salts in this case was the highest.

Unlike as observed for silver doped samples, Cu tends to oxidize easily in an environment containing Fe ions.

## 7.2.10.7. Calorimetric measurement

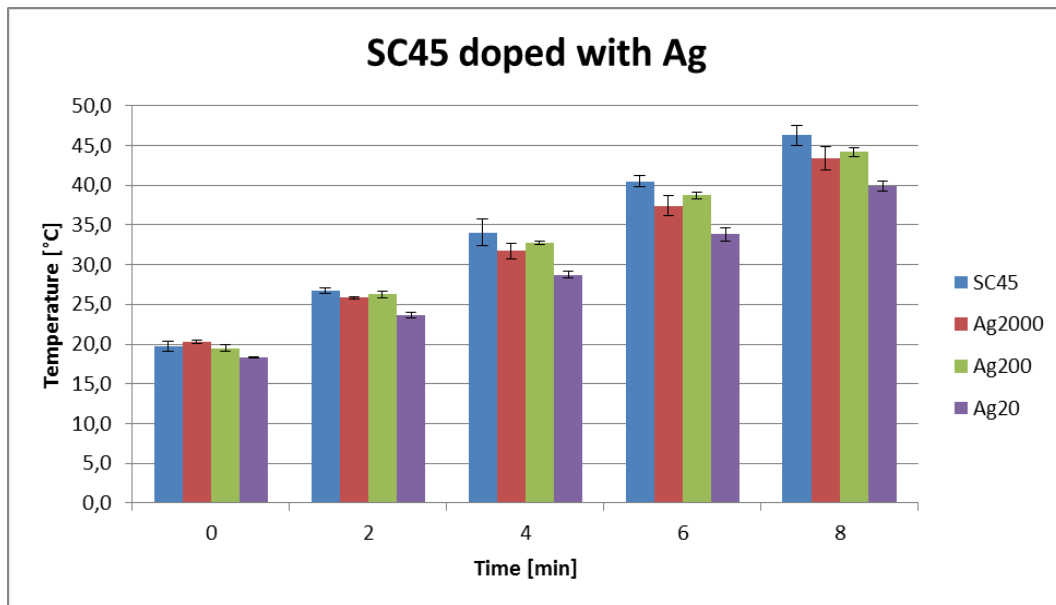


Figure 7.78: Calorimetric test on SC45 doped with silver

Figure 7.78 shows the heating of the powders of SC45 doped with silver. The temperature of the SC45 increases always more than all silver doped samples, thus silver does not induce improvements in the ability of heat generation. SC45 Ag2000 and SC45 Ag200 have similar behaviour and they maintain below the control. SC45 Ag20 sample presents a slight decrease in heating at all-time points than the other samples. However after 8 minutes, the average temperature recorded, on three repeated tests, is reported to be between 40°C and 45°C. This confirms the possibility of the hyperthermia application for these magnetic materials.

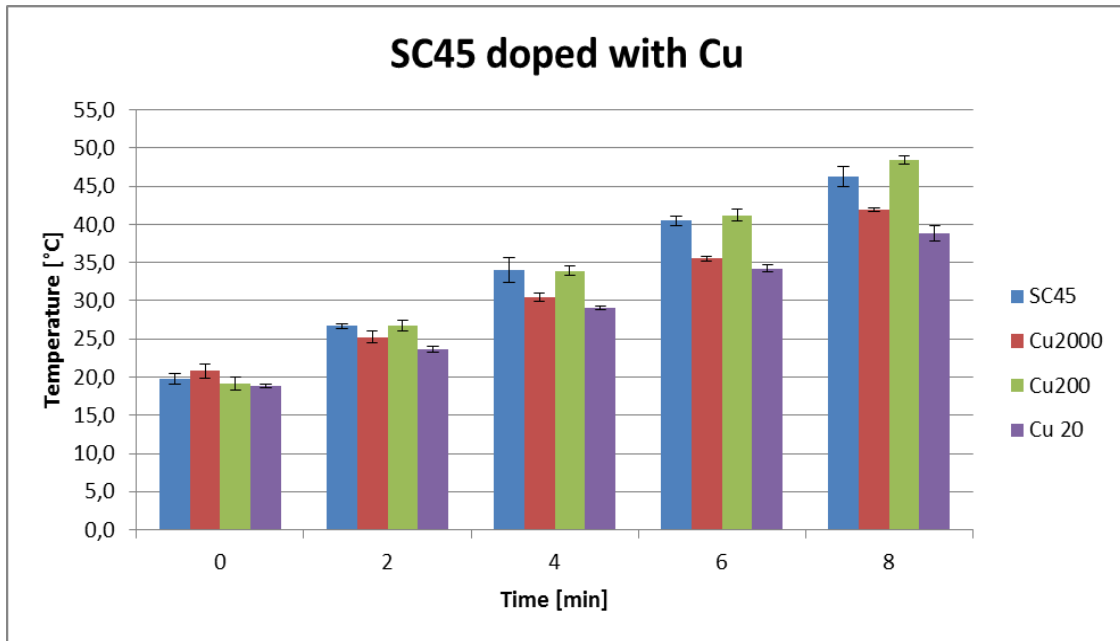


Figure 7.79: Calorimetric test on SC45 doped with copper

Figure 7.79 shows the results of the calorimetric measurements on samples of SC45 doped with copper. As for silver, the heating were not higher than the control sample except for the Cu200 that exceeds of 4.7% SC45 at 8 minutes. Cu200 has the same heating behavior of SC45. While Cu20 and Cu2000 show a temperature increase lower than the control. This preliminary calorimetric investigation confirm a non significantly difference among the samples. However further investigation will need for understand the static magnetic behavior of these specimens .

#### 7.2.10.8. Antibacterial tests

The antibacterial properties of Ag and Cu doped glass-ceramics were evaluated by the inhibition halo test (Kirby Bauer test) using a standard *Staphylococcus aureus* strain.

The samples were produced using 200 mg of silver/copper-doped SC45 powders uniaxially pressed at 4 tons for 10 seconds in order to prepare disks of a diameter of 1 cm and a tickness of 0,5 mm as reported in chapter 5 Material and Methods.

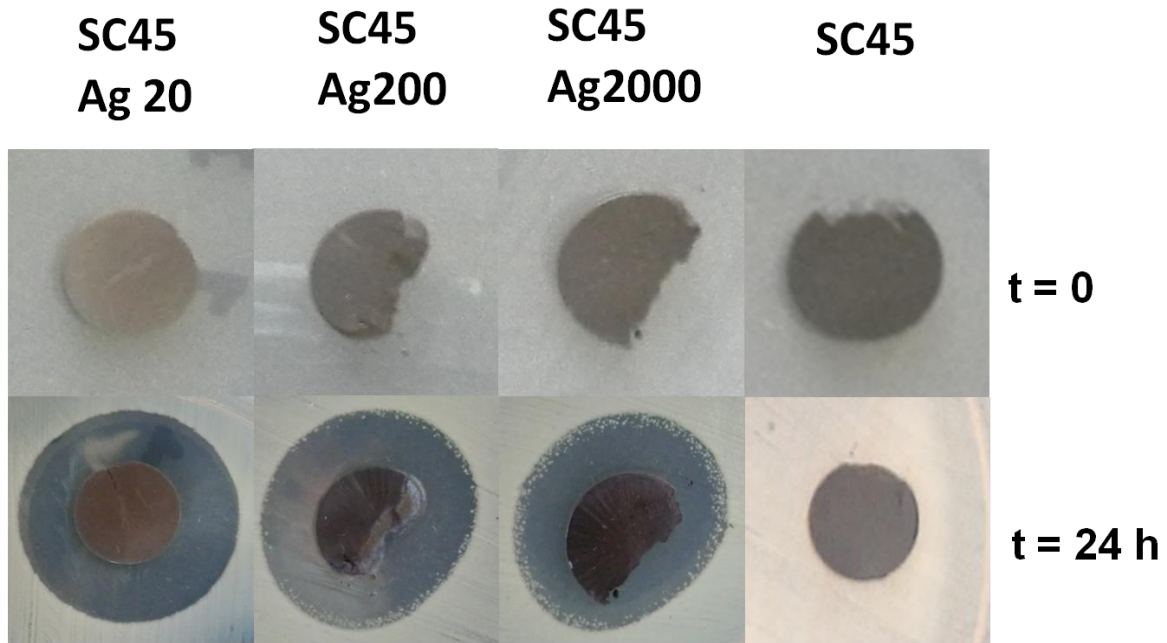


Figure 7.80: Antibacterial test on SC45 doped with silver

All samples containing Ag produced a significant inhibition halo. SC45 Ag2000 and SC45 Ag200 samples show the presence of a double halo: a first well defined in direct contact with the sample surface and a second one (more peripheral) in which some colonies begin to proliferate. This behavior is due to the fact that to a certain extent of the agar the amount of released silver is able to stop the bacterial proliferation, while in the second halo the silver amount decrease and some bacterial colonies began to proliferate

SC45 Ag20 sample produces a uniform halo. In fact the silver concentration decreases away from the sample until reaching, for Ag 200 and 2000, a value for which some bacterial colonies begin to survive and proliferate. Ag 20 has not produced any discontinuity in the halo.

The antibacterial effect is conferred by silver present in various forms in the glass .

Samples identification	Mean diameter of inhibition halo after 24h at 37°C in contact with staphylococcus aureus [mm]
SC45	0
SC45 Ag2000	5
SC45 Ag200	5,5-6
SC45 Ag20	6,5-7

Table 7.10: Mean diameter of inhibition halos of SC45 doped with silver

## Results and Discussion Antibacterial characterization of SC45

Table 7.10 reports the mean diameter of inhibition halo produced by magnetic glass ceramic doped with silver. As expected, increasing the silver concentration into the glass-ceramic the diameter of the halo increases.

The antibacterial effect obtained for these samples indicates a contribution of both the silver ion present in the glassy network and the nano-metric precipitates that were seen in all three syntheses by FESEM-EDS and XRD. In fact, despite the concentration of silver in the glass ceramic are very different one from each other, all of them produced very wide and sharp halos, this indicates that a large contribution to the antibacterial effect was given by silver present in all samples in its different forms. SC45 Ag 2000 for example does not present a very high quantity of silver in the glass network, but it presented various precipitates of metallic silver, which contributes to the halo generation.

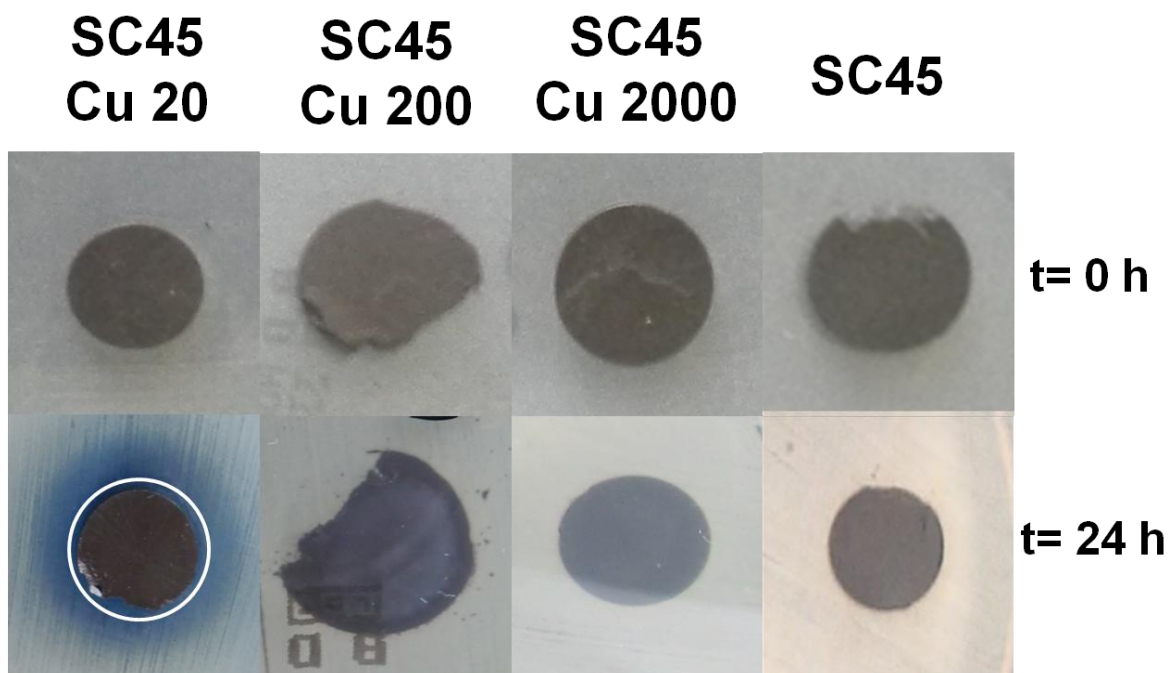


Figure 7.81: Antibacterial test on SC45 doped with copper

The antibacterial effect of copper is less evident than that observed for silver (figure 7.81). In particular, only around the SC45 Cu20 sample is observed the presence of about 1 mm inhibition halo (see figure 7.81 and table 7.11). In this sample is also observed a blue halo due to the diffusion of Cu on the bacterial plate, however only next to the sample the concentration of Cu is such high to inhibit the bacterial proliferation.

The samples SC45 Cu 200 and SC45 Cu 2000 do not have antibacterial effect, the concentration of copper is too low to inhibit bacterial proliferation.

## Results and Discussion Antibacterial characterization of SC45

<b>Samples identification</b>	<b>Mean diameter of inhibition halo after 24h at 37°C in contact with staphylococcus aureus [mm]</b>
SC45	0
SC45 Cu2000	0
SC45 Cu200	0
SC45 Cu20	1-1,5

**Table 7.11: Mean diameter of inhibition halo tests of SC45 doped with copper**

Table 7.11 reports the mean diameter of the inhibition halo (when observable) for SC45 Cu2000, SC45Cu200 and SC45 Cu20.

### 7.2.10.9. Bioactivity tests

To evaluate the result of the bioactivity test, the trends of the solutions pH, containing samples of different compositions, have been compared. To verify the reactivity in SBF and the possible nucleation of silica gel or hydroxyapatite, the samples were analyzed using X-Ray Diffraction (XRD) and Scanning Electron Microscope (SEM / EDS).

In table 7.12 the identification of all samples :

<b>Sample identification</b>	<b>Acronyms Explanation</b>
SC45	Control sample before SBF treatment
SC45-3W	Control samples after 3 weeks in SBF
SC45-4W	Control samples after 4 weeks in SBF
SC45 Ag2000-3W	Low silver concentration samples after 3 weeks in SBF
SC45 Ag2000-4W	Low silver concentration samples after 4 weeks in SBF
SC45 Ag200-3W	Medium silver concentration samples after 3 weeks in SBF
SC45 Ag200-4W	Medium silver concentration samples after 4 weeks in SBF
SC45 Ag20-3W	High silver concentration samples after 3 weeks in SBF
SC45 Ag20-4W	High silver concentration samples after 4 weeks in SBF
SC45 Cu2000-3W	Low copper concentration samples after 3 weeks in SBF
SC45 Cu2000-4W	Low copper concentration samples after 4 weeks in SBF

## Results and Discussion Antibacterial characterization of SC45

SC45 Cu200-3W	Medium copper concentration samples after 3 weeks in SBF
SC45 Cu200-4W	Medium copper concentration samples after 4 weeks in SBF
SC45 Cu20-3W	High copper concentration samples after 3 weeks in SBF
SC45 Cu20-4W	High copper concentration samples after 4 weeks in SBF

Table 7.12: Sample identification for in vitro bioactivity tests

### 7.2.10.9.1. Evaluation of SC45 surface before and after bioactivity test

In order to study the surface reactivity of the SC45 during soaking in SBF, the variation of the % of the elements potentially involved in the bioactivity process was evaluated, comparing the trend of sodium, silicon, phosphorus, calcium and iron before the treatment (control), after three weeks in SBF (3W) and after 4 weeks (4W) in SBF.

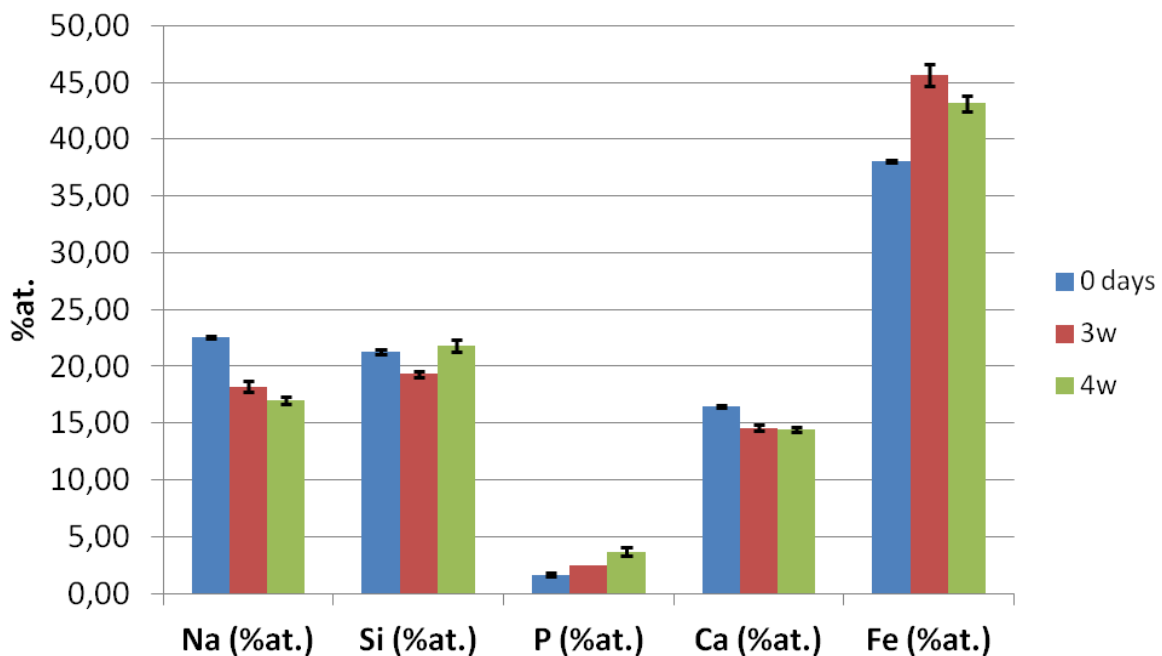


Figure 7.82: % atomic variation of the elements on the SC45 surface before and after in vitro bioactivity test.

The values reported in figure 7.82 are the average calculated from three area EDS analysis on SC45 before and after three and four weeks in SBF. It can be observed that sodium (Na) decreases both after three and four weeks in SBF, silicon (Si) is slightly reduced after three weeks and then returns to a value close to the starting point, phosphorus (P) increases in time, calcium is slightly reduced

## Results and Discussion Antibacterial characterization of SC45

but it is stable at three and four weeks, while iron (Fe) increases after three weeks then slightly decreases at four. This trend is in agreement with the bioactivity process: sodium is typically released in the solution and replaced with hydroxyl ions, silica increase at 4 weeks due to the presence of silica gel formation. The concept of bioactivity is explained in chapter 2 .

The phosphorus increases in 4 weeks of 122% , this is justifiable according to the process of bioactivity which provides precipitation of this ion on the surface of the glass-ceramic even if not completely crystallized as hydroxyapatite.

The EDS analysis of area shows more iron in the exposed glass particles at 3 weeks because the development of ionic exchange-glass solution has partially dissolved the glassy matrix. The reduction at 4 weeks can be related to the formation of a silica and phosphate gel layer that partially covered the magnetite particles previously exposed.

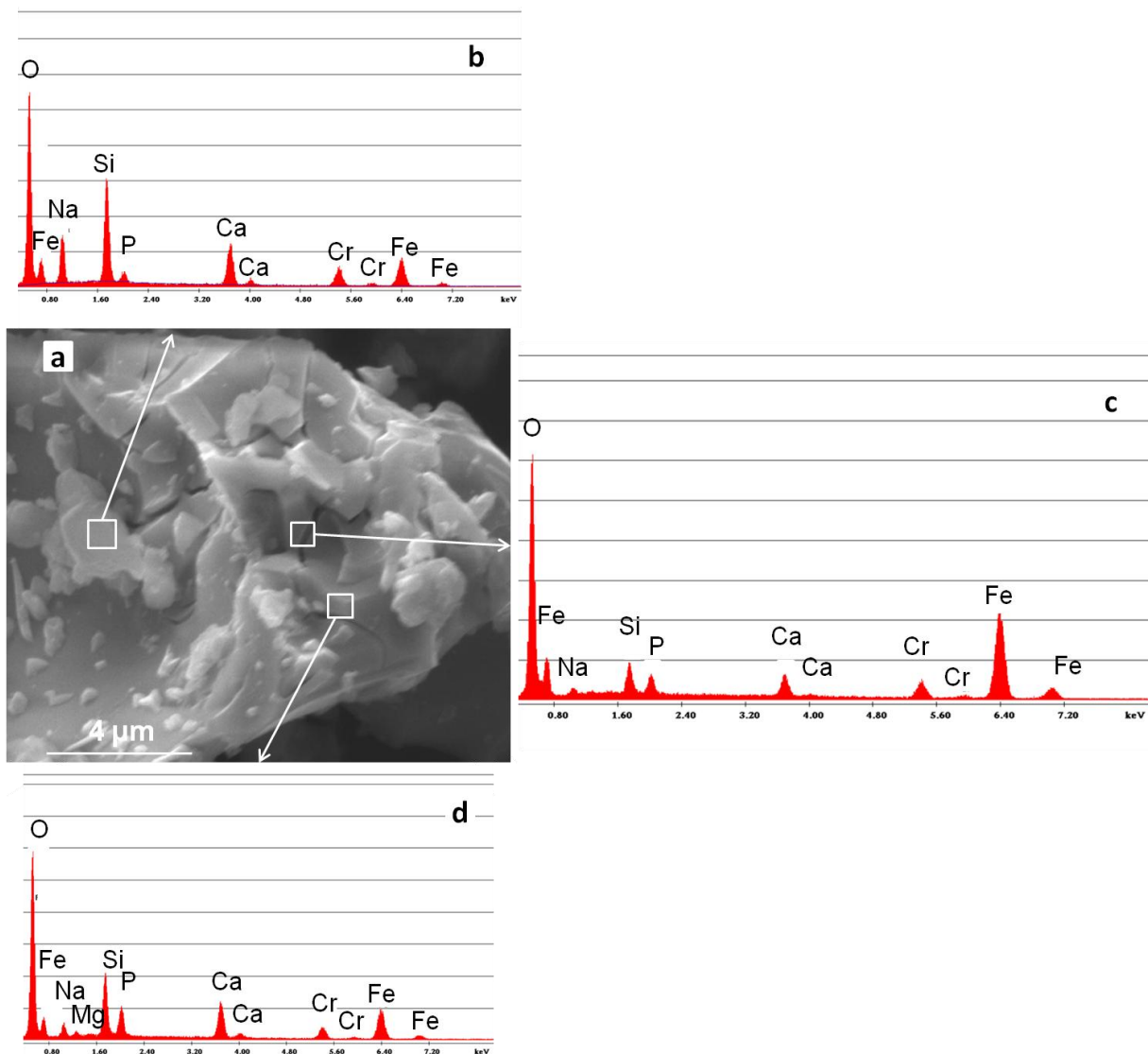


Figure 7.83: Morphology and EDS analysis on different sample areas of SC45 after 4 weeks in SBF.

## Results and Discussion Antibacterial characterization of SC45

Figure 7.83 reports SC45 particles after 4 weeks of soaking in SBF. On this surface various details with different morphology can be noticed and they have been analyzed; the respective EDS spectra are reported in figure 7.83b-c-d.

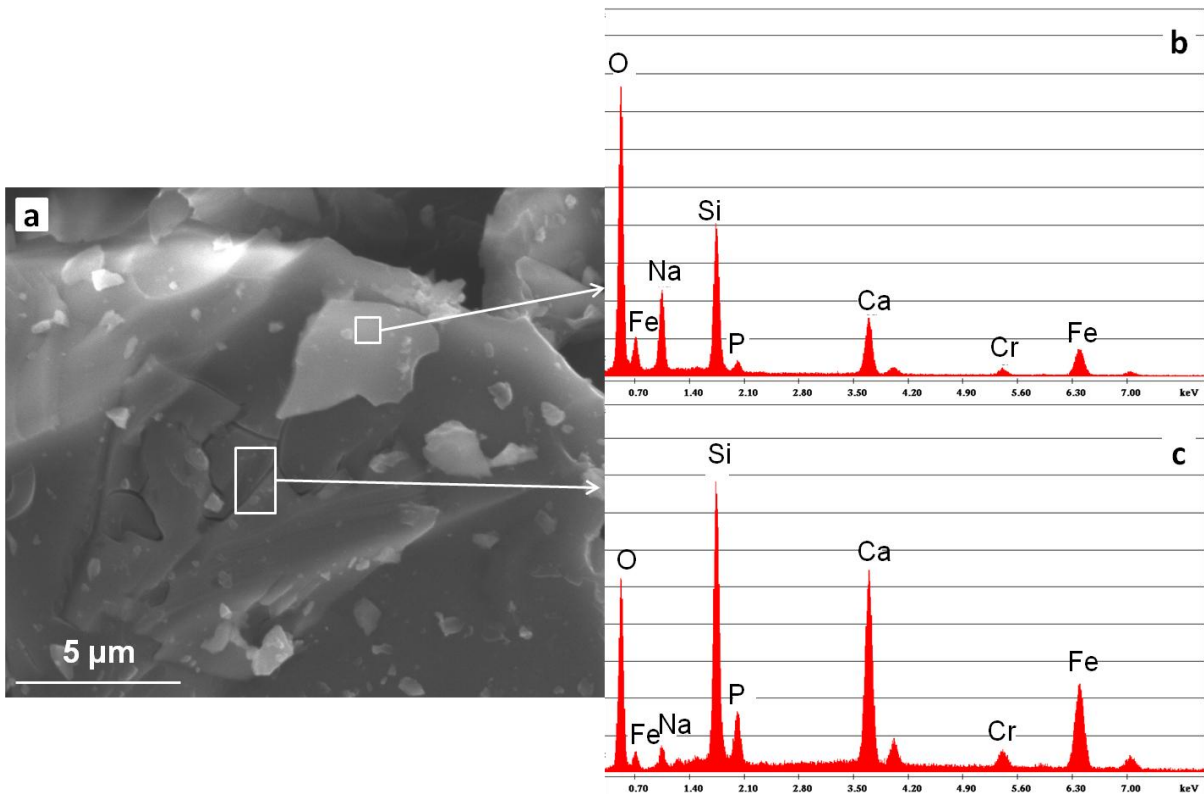


Figure 7.84: Morphology and EDS analysis on different sample areas of SC45 after 3 weeks in SBF.

Figure 7.84 reports a morphological and compositional analysis of SC45 sample after 3 weeks in SBF. In figure 7.84a two different traces of the bioactivity process are present: the first is a flat layer of silica gel enriched by calcium as confirmed by EDS analysis (figure 7.84b). The second analyzed area evidences high peaks of silicon calcium and phosphorus which can suppose the presence of a silica gel layer enriched in Ca and P (Figure 7.84c).

The cracks observed in the images 7.48a are a common morphological feature for silica-gel grown on bioactive material.

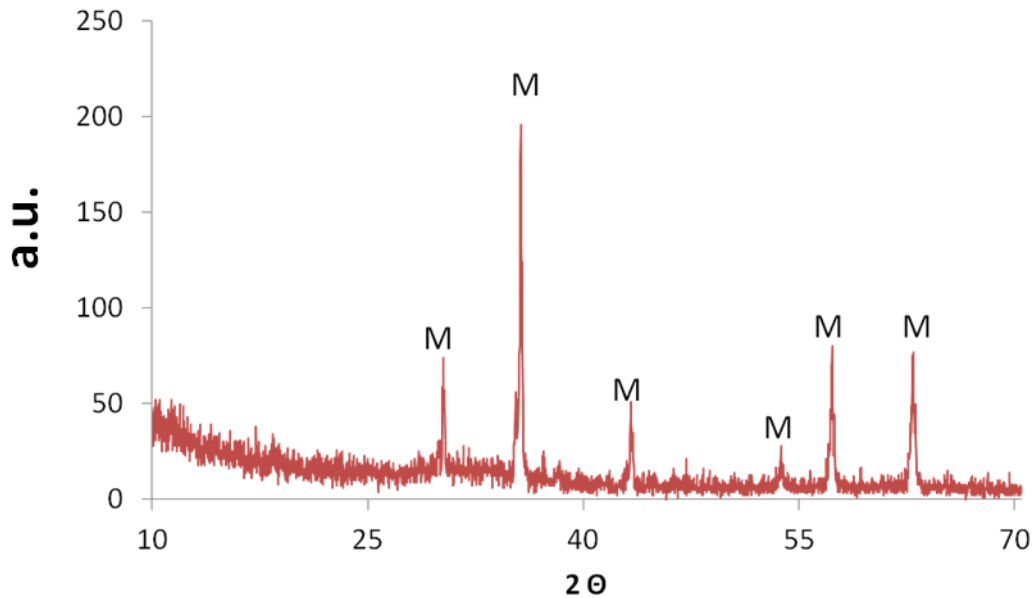


Figure 7.85: XRD analysis of SC45 - 4W

Figure 7.85 reports the XRD analysis of SC45 after 4 weeks in SBF solution. The pattern reports the typical peaks of magnetite without the presence of crystallized calcium phosphate or hydroxyapatite as confirmed by the morphology analysis.

#### 7.2.10.9.2. Bioactivity of SC45 doped with silver

The bioactivity characterization on SC45 doped with silver was performed at 3 and 4 weeks of immersion in SBF with a scanning electron microscopy of the powder surface, compositional analysis (EDS) and x-ray diffraction (XRD) for the glass ceramic with all the different of silver concentration .

Figure 7.86 reports the trend of the pH measured in the different solutions during soaking in SBF. The curve was obtained by interpolating the average values obtained from each sample and taking into account the respective standard deviations.

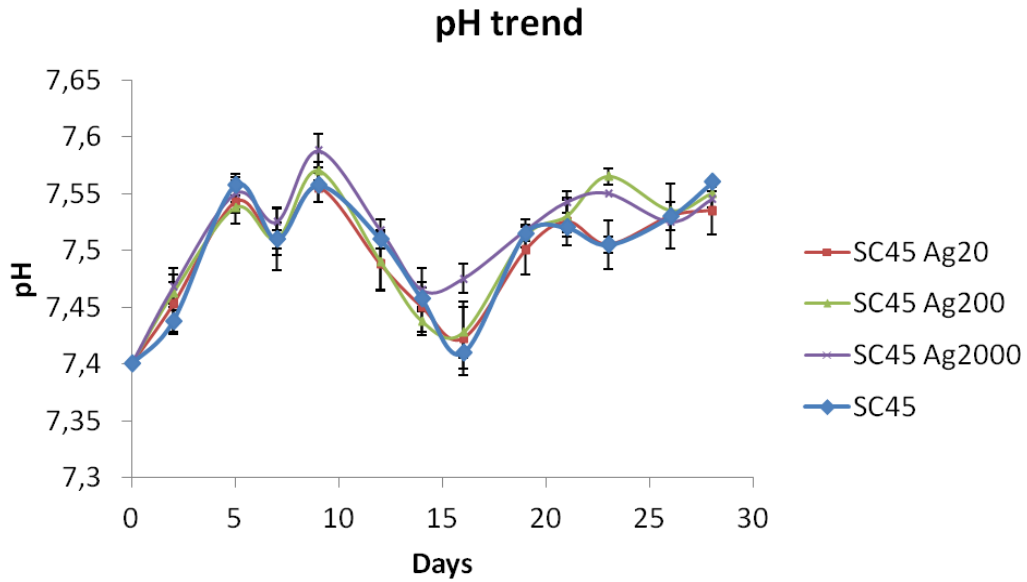


Figure 7.86: pH variation vs time for the silver-doped glass-ceramics compared to the un-doped SC45, during soaking in SBF.

Any significant variation in the pH value during the test can be notice between the different compositions of silver-doped glass-ceramic if compared to the control (SC45). The pH is kept almost stationary and oscillates between 7.4 (starting value, physiological pH ) and 7.6. The recorded values fluctuate within the range considered acceptable by human cells (7.0-7.8).

The variability of the measurements is connected with the ion exchange of the samples bioactivity process where the silver ions do not seem to have an influence.

## Results and Discussion Antibacterial characterization of SC45

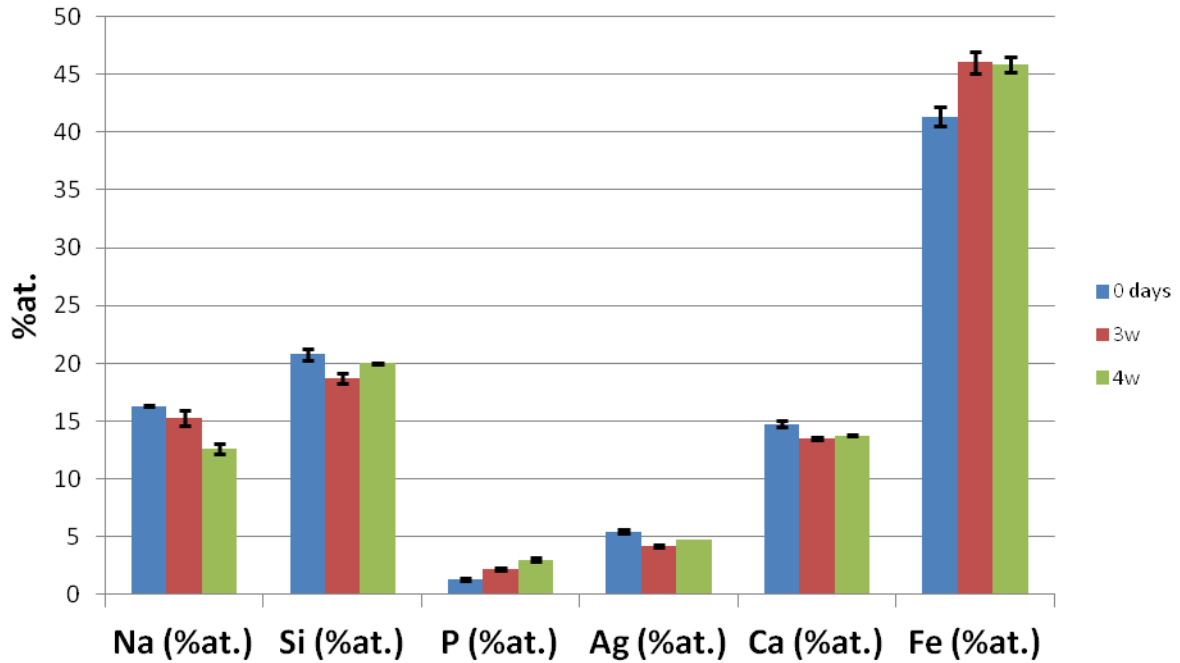


Figure 7.87: % atomic variation of the elements on the SC45 Ag 2000 surface before and after in vitro bioactivity test.

The average data obtained from EDS analysis present a sodium decrease during time (trend similar to SC45). Silicon presents a decreasing trend. Phosphorus grows during time, silver undergoes a few changes as well as calcium, while iron increases for the entire duration of the test. The trend of iron could be justified by an increased exposed surface area of magnetite, due to a dissolution of the glass matrix..

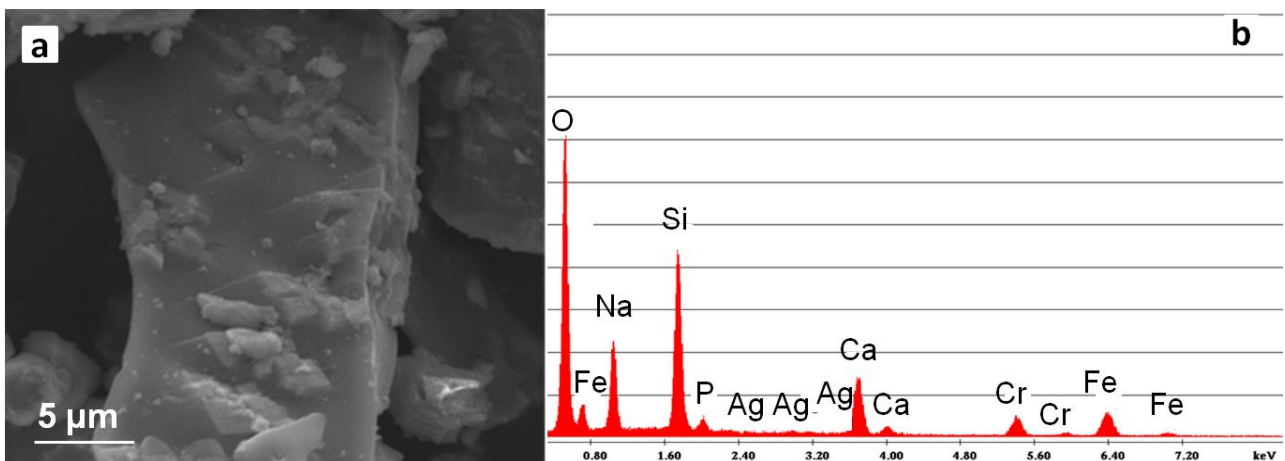


Figure 7.88: SEM morphology (a) and EDS analysis (b) of SC45 Ag2000 after 4 weeks in SBF

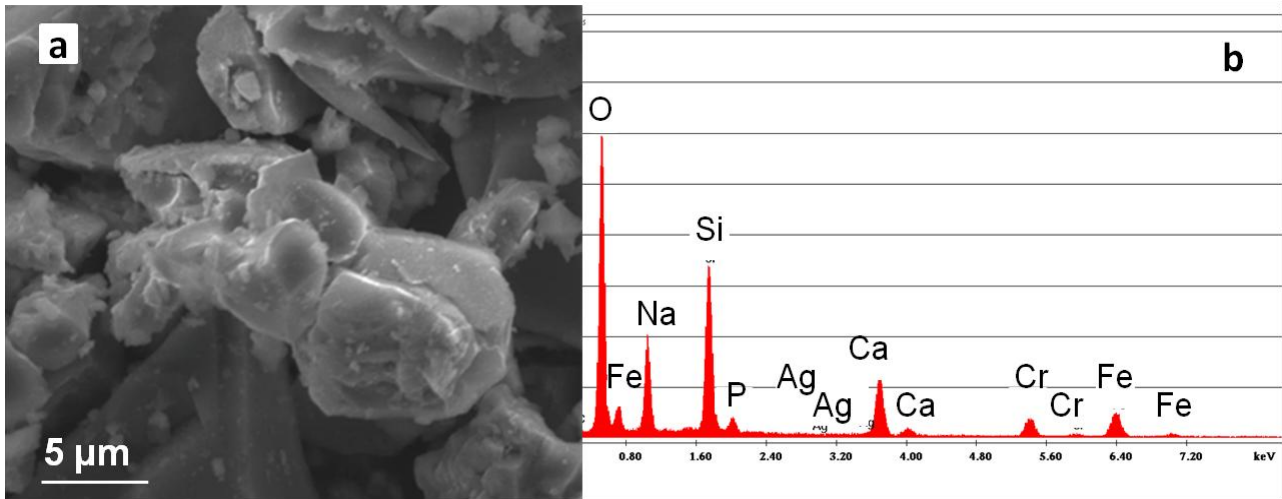


Figure 7.89: SEM morphology (a) and EDS analysis (b) of SC45 Ag2000 after 4 weeks in SBF

Chemical Element	EDS analysis	EDS analysis
	% atomic (Fig. 7.88)	% atomic (Fig 7.89)
Na	27,1	28,5
Si	36,2	34,7
P	2,6	3,5
Ag	0,7	0
Ca	16,3	16,1
Fe	17,1	17,1

Table 7.13: Local EDS analysis of SC45 Ag2000-4W particles

In table 7.13 the morphology and the EDS analysis of SC45 Ag2000-4W particle in fig. 7.88 and in figure 7.89 are quite similar. The comparison between two local EDS analysis does not present any difference. This result confirms the hypothesis of the development of an amorphous silica-calcium phosphate layer during the bioactivity mechanism of the glass ceramic matrix without generating hydroxyapatite in a crystalline form.

## Results and Discussion Antibacterial characterization of SC45

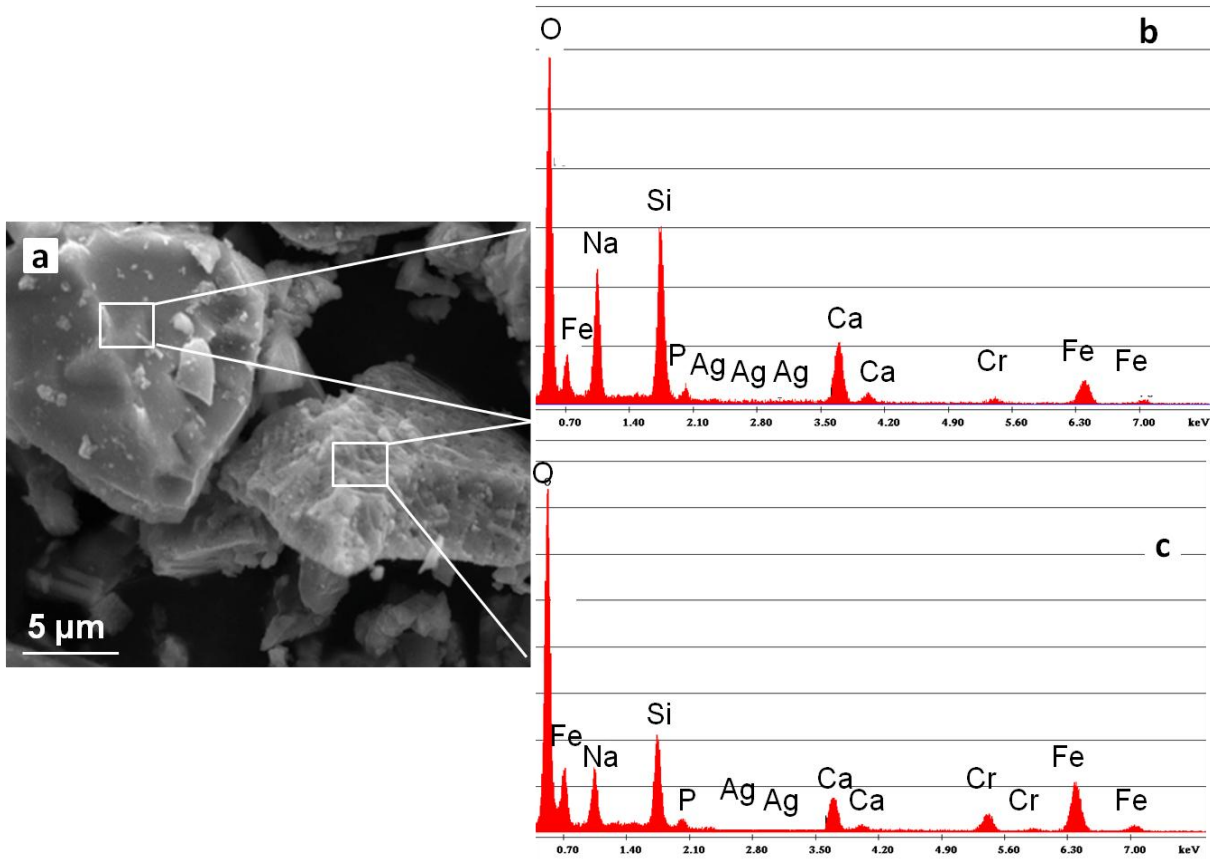


Figure 7.90: SEM morphology of SC45 Ag 2000 after 4 weeks in SBF

Chemical Element	EDS analysis	
	% atomic Fig. 6.100b	% atomic Fig. 6.100c
(Na)	33,5	25,4
(Si)	32,8	22,9
(P)	2,1	2,3
(Ag)	0	0,4
(Ca)	15,9	10,8
(Fe)	15,7	38,2

Table 7.14: Local EDS analysis of SC45 Ag2000-4W particle

In table 7.14 the EDS analysis performed on the SC45 Ag2000-4W particle in figure 6.90 b shows a high amount of sodium, silicon and calcium in respect to those reported figure 6.90c. On the other hand, figure 6.90c shows a high amount of iron on the powder surface.

## Results and Discussion Antibacterial characterization of SC45

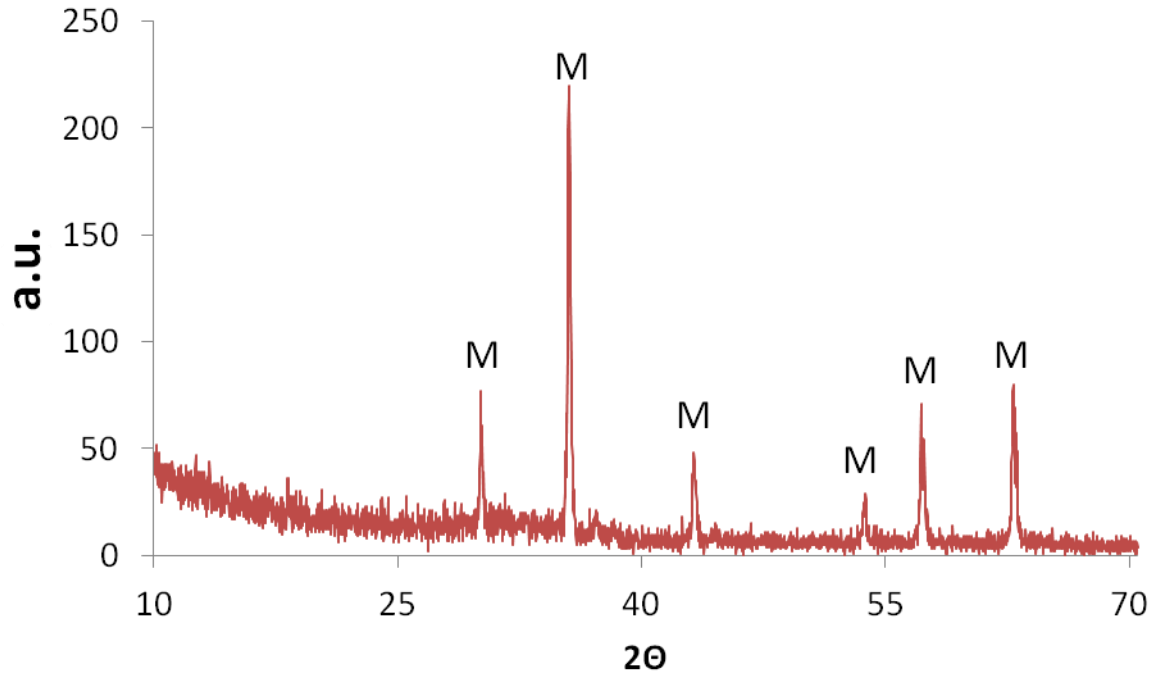


Figure 7.91: XRD analysis on SC45 Ag2000-4W

Figure 7.91 reports the XRD pattern performed on SC45 Ag2000 after 4 weeks in SBF sample. The only signals are referred to magnetite, any signal of hydroxyapatite is visible..

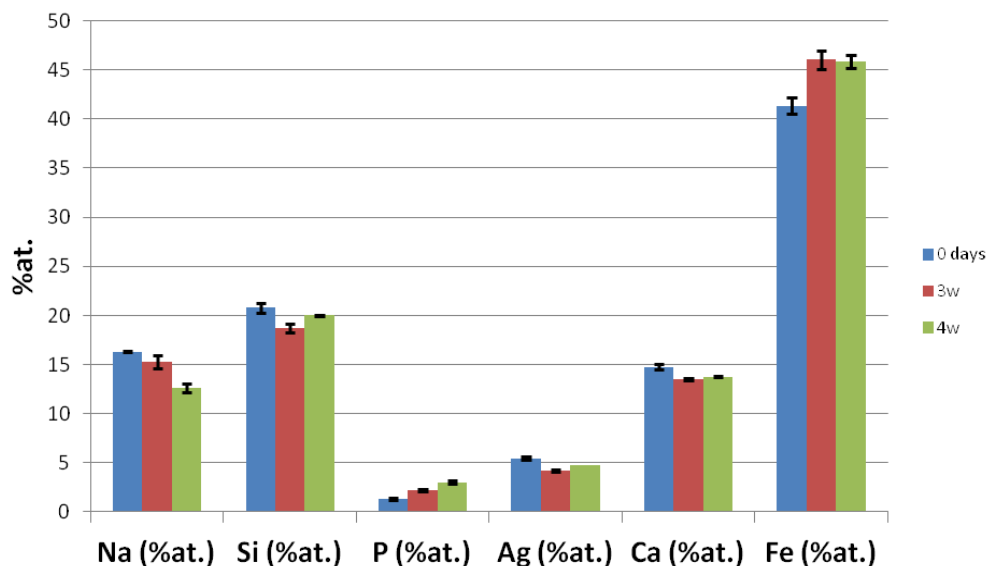


Figure 7.92: % atomic variation of the elements on the SC45 Ag 200 surface before and after in vitro bioactivity test.

From the values of mean area EDS analysis in figure 7.92 it can be observed that the amount of sodium decreases at each time point (as for SC45), silicon slightly decreases after three weeks and then slightly increases (with a trend similar to that of SC45), phosphorus increases after three and four weeks similarly to SC45 and SC45 Ag20. Silver amount initially decreases and then seems to

## Results and Discussion Antibacterial characterization of SC45

stabilize, similarly to SC45Ag20. The calcium content follows a trend very similar to that observed for SC45, while iron increases after three weeks and then it remains constant.

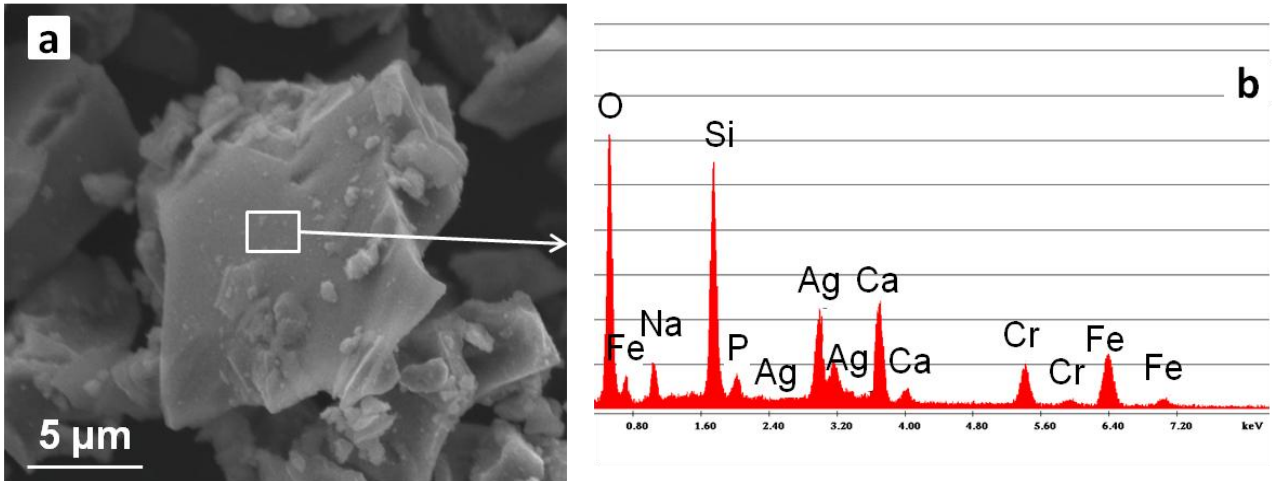


Figure 7.93: SEM morphology and EDS analysis of SC45Ag 200 after 4 weeks in SBF

The EDS analysis on a particle of SC45 Ag200-4W after soaking in SBF for 4 weeks (figure 7.93) reports a high peak of silicon respect to the other elements. In agreement with this observation, even local EDS analysis confirms an increase of silicon respect to the mean area value.

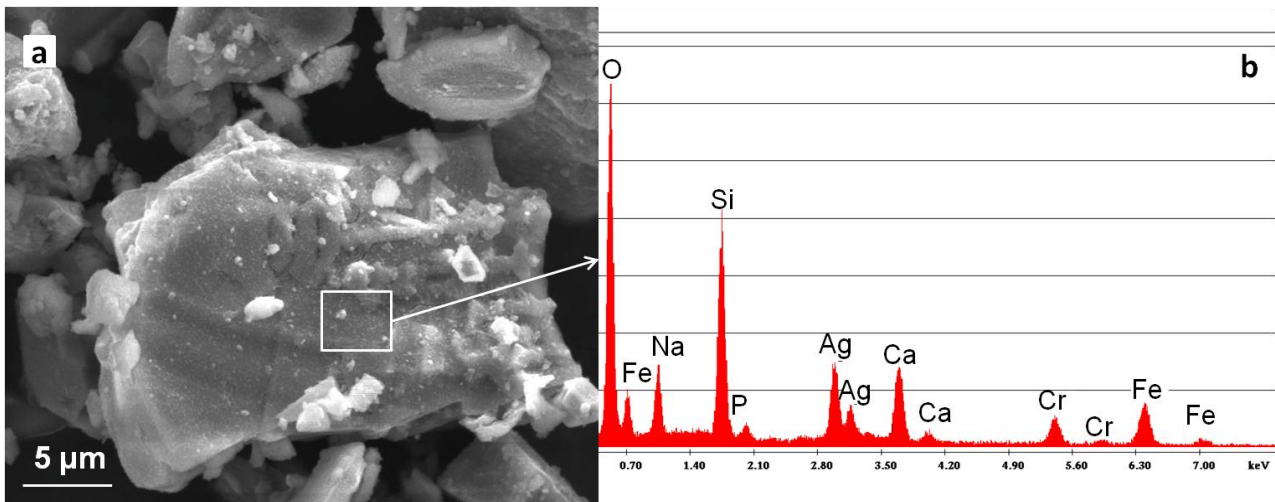


Figure 7.94: SEM morphology (a) and EDS analysis of SC45 Ag 200 after 4 weeks in SBF (b)

The SC45 Ag200-4W sample, in figure 7.94a, shows very fine and small particles on the surface of the glass-ceramic. A local EDS analysis was performed, as it can be seen in figure 7.94b the peak of silicon is higher respect to the others. Probably it is formed a layer of silica gel on the glass ceramic particle.